Macromolecular Bioscience
www.mbs-journal.de

Development of BDNF/NGF/IKVAV Peptide Modified and Gold Nanoparticle Conductive PCL/PLGA Nerve Guidance Conduit for Regeneration of the Rat Spinal Cord Injury

Ilyas Ozcicek, Nese Aysit, Zeynep Balcikanli, Nilufer Ulas Ayturk, Asel Aydeger, Gulsena Baydas, Mehmet Serif Aydin, Esra Altintas, and Umit Can Erim*

Spinal cord injuries are very common worldwide, leading to permanent nerve function loss with devastating effects in the affected patients. The challenges and inadequate results in the current clinical treatments are leading scientists to innovative neural regenerative research. Advances in nanoscience and neural tissue engineering have opened new avenues for spinal cord injury (SCI) treatment. In order for designed nerve guidance conduit (NGC) to be functionally useful, it must have ideal scaffold properties and topographic features that promote the linear orientation of damaged axons. In this study, it is aimed to develop channeled polycaprolactone (PCL)/Poly-D,L-lactic-co-glycolic acid (PLGA) hybrid film scaffolds, modify their surfaces by IKVAV pentapeptide/gold nanoparticles (AuNPs) or polypyrrole (PPy) and investigate the behavior of motor neurons on the designed scaffold surfaces in vitro under static/bioreactor conditions. Their potential to promote neural regeneration after implantation into the rat SCI by shaping the film scaffolds modified with neural factors into a tubular form is also examined. It is shown that channeled groups decorated with AuNPs highly promote neurite orientation under bioreactor conditions and also the developed optimal NGC (PCL/PLGA G1-IKVAV/BDNF/NGF-AuNP$_{50}$) highly regenerates SCI. The results indicate that the designed scaffold can be an ideal candidate for spinal cord regeneration.

1. Introduction

Spinal cord injuries (SCI), which are quite common in the society have serious effects on the life quality, social and economic conditions of the patients. Global prevalence of SC damages has increased from 236 to 1298 cases (per million population) over the past 30 years. The estimated global rate of SCI is in the range of 250 000 to 500 000 each year, and current clinical treatment approaches are very limited.[1,2] Although there is a great regeneration capacity for peripheral nervous system (PNS) injuries, the neural regeneration potential is very limited for central nervous system (CNS) damages due to inhibitory environment of the CNS and functional recovery is extremely difficult.[3,4] Cystic glial scar tissue that develops as a result of neural damage constitute an important physical and chemical barrier for functional nerve regeneration.[5] Damaged neurons must survive and cellular axons must extend along linear lines in parallel for a functional nerve repair. In addition, there is a big need for myelination and regeneration of functional synapses.[3]

Autografts are still preferred as a gold standard in the nerve treatments. Autografts are taken from the less functional nerve

I. Ozcicek, N. Aysit, Z. Balcikanli, A. Aydeger, G. Baydas, M. S. Aydin, E. Altintas, U. C. Erim
Research Institute for Health Sciences and Technologies (SABITA)
Istanbul Medipol University
Istanbul 34810, Turkey
E-mail: iozcicek@medipol.edu.tr

I. Ozcicek, N. Aysit
Department of Medical Biology
School of Medicine
Istanbul Medipol University
Istanbul 34815, Turkey

N. U. Ayturk
Department of Histology and Embryology
Faculty of Medicine
Çanakkale Onsekiz Mart University
Canakkale 17020, Turkey

A. Aydeger, G. Baydas, E. Altintas
Graduate School of Health Sciences
Istanbul Medipol University
Istanbul 34815, Turkey

G. Baydas
Department of Physiology
School of Medicine
Istanbul Medipol University
Istanbul 34815, Turkey

U. C. Erim
Department of Analytical Chemistry
School of Pharmacy
Istanbul Medipol University
Istanbul 34815, Turkey

The ORCID identification number(s) for the author(s) of this article can be found under https://doi.org/10.1002/mabi.202300453

DOI: 10.1002/mabi.202300453

parts of the person and placed on the injured area; However, it requires a second surgical procedure and the limited length of the nerve removed is another problem. The clinical functional gain in the autologous grafts is ≈80%, and this rate is considerably lower, especially in the long defects.[6–9] Allografts taken from cadavers are an alternative approach. Although it is an advantage that it can be taken from where it is needed and at the desired length, it requires a long treatment period of 18 months to suppress the immune response. Allografts also have some disadvantages such as the risk of secondary infection and tumor development.[10–12] The current clinical treatment of SCI is high-dose methylprednisolone (MP) combined with surgical methods. MP is a type of glucocorticoid and acts through various mechanisms such as inhibition of lipid peroxidation and prevention of inflammation by reducing cytokine release. MP is only effective if given within the first eight hours following injury, after which it may causes more harm than good, additionally it is a treatment with highly undesirable side effects. Systemic drug delivery also faces many challenges, such as renal clearance, limited drug circulation time, and drug degradation.[13,14]

In the field of nerve tissue engineering, intensive work is being done to develop alternative nerve guidance channels with the new techniques offered by nanotechnology and materials science; However, an ideal neural tissue scaffold that can mimic the natural extracellular matrix (ECM) has an intraluminal channeled structure, appropriate micro/nano patterning, and also can support and guide neural cells which has not yet been fully developed.[15] Biomaterials used in the treatment of nerve injuries with tissue engineering approaches can be synthetic, natural, or hybrid structures obtained by mixing both in certain proportions.[16] The biggest advantage of natural polymers is that they can better mimic the ECM environment and interact better with cells. On the other hand, the mechanical properties of synthetic polymers can be controlled better. In addition, synthetic polymers have other important advantages such as hydrophilicity, biodegradability, elasticity, mechanical strength.[17] The biocompatibility of an ideal scaffold is an extremely important issue, which promotes cell adhesion, migration, and proliferation.[18] It is known that topographic features have a positive contribution to axonal orientation and the physical guidance provided to the axons is critical for nerve repair.[3] Neural cells have a highly polarized shape, with the cell body at one end and the axon at the other end. A significant axonal orientation must be achieved for functional nerve regeneration. Topographic patterns created on the biomaterial surfaces in various shapes (such as micro/nano fibers, grooves, filaments, strips, pillars, conduits) promote the orientation of axons by providing contact guidance.[19,20] Axonal orientation is a result of the rearrangements of microtubules and actin proteins within the growth cone of the axons following the adhesion of neural cells to the biomaterial surface.[21] Neural cells require aligned micro/nanostructures to perform signal transduction functions. Controlled topographies created on the designed scaffold surfaces direct the growth of dendrites and axons for signal transmission. Many techniques such as electrospinning, photolithography, laser-induced patterning, electron beam lithography, bioprinting, magnetic orientation, and isoelectric focusing are used to create topographies that will induce axonal growth on biomaterial surfaces;[22–28] Thus, topographic patterns in the neural scaffolds to be designed are very important to ensure effective neural regeneration.

Polycaprolactone (PCL) is a biodegradable, biocompatible, low-cost, non-toxic, elastic, mechanically strong and slow-degrading FDA approved polymer.[29] PCL has an adjustable degradation kinetics and mechanical property, and it can be easily shaped.[30,31] In the literature, a wide range of neural cell types (DRG primary sensory neurons, Schwann cells and primary cortical neurons, PC12 cells, C17.2 neural stem cells and embryonic stem cells) have been studied using PCL-based micro/nano fibers obtained by electrospinning technique. In particular, aligned micro/nano fibers used in the literature studies have been shown to support axon/neurite development along the parallel lines, and PCL has been shown to be highly biocompatible for various neural cells.[32–44]

Polylactic-co-glycolic acid (PLGA), one of the most preferred biodegradable synthetic polymers in tissue engineering applications, is a copolymer of polylactic acid (PLA) and polyglycolic acid (PGA).[45] PLGA, an FDA-approved biodegradable polymer, has superior mechanical properties and non-toxic degradation products.[46] Despite the popularity and widespread use of PLGA in the area of tissue engineering, its applications in the neural tissue engineering field are limited and still not at the desired level. In the literature, PLGA-based scaffolds with various properties were shown in some studies to investigate neural cell responses. In these studies, it has been shown that narrower channeled biomaterials promoted neurite elongation/orientation, and aligned fibrous scaffolds increased axonal guidance and neural cell differentiation.[47–51] In a study, it was shown that surface topography is an important parameter for cell differentiation and excessive surface roughness inhibits cell differentiation, as a result of glia/neuron co-culture on the micro/nano-patterned Si surfaces with laser irradiation in PLGA material.[52] In another study, antioxidant salidroside molecule was used together with PLGA as a neural biomaterial. It has been shown that the designed scaffold supports Schwann cell proliferation/development, and also greatly promotes neural regeneration as a result of its combined use in the sciatic nerve damage.[53] There are several studies in the literature where PLGA is used together with various conductive materials (such as electroactive $FeCl_3$ doped poly-3-hexylthiophene, C-nanotube, graphene, gold/chitosan nanoparticle) within the scope of neural tissue engineering. In these studies, the behaviors of various neural cells were examined on the designed conductive PLGA biomaterials, and it was shown that the cell adhesion, proliferation, development, differentiation, and neurite extension increased significantly.[54–57]

Neurotrophic factors are the biomolecules that have very important roles in the survival, migration, development, differentiation of different neural cells, and therefore in nerve regeneration. They have also critical roles in establishing synaptic connections between neurons and regulating neural signal transmission.[58] These molecules which provide growth, differentiation, and cell adhesion, can be covalently attached to the biomaterial surfaces, as well as easily bonded by physical interactions.[59] Numerous studies have shown that neural growth factor (NGF) supports the survival of neurons and promotes nerve regeneration; Also, NGF molecule promotes the differentiation of neural stem cells into mature neuronal phenotypes. In addition, NGF affects the migration of oligodendrocytes in the CNS and promotes neurite

Table 1. Main characteristic properties of synthesized AuNP groups.

Groups	Hydrodynamic diameter [nm]	Polydispersity index	UV–Visible peak [nm]	Zeta potential [mV]
$AuNP_{20}$	20.66 ± 0.15	0.16	521	−51.72
$AuNP_{50}$	50.83 ± 0.18	0.082	536	−29.36

elongation.[60,61] Brain-derived neurotrophic factor (BDNF) has been the best characterized neurotrophic factor for neuronal viability, differentiation, survival, and synaptogenesis until today. It is known that BDNF has a very short half-life (≈30 min.) following systemic injection; Therefore, it is critical that BDNF must be found in the injured area in sufficient time and concentration for a functionally adequate neural regeneration.[62,63] Extracellular matrix (ECM) biomolecules are frequently preferred to promote cellular adhesion and development.[34,64] Peptide motif sequences derived from these proteins have also well studied in the recent years. The advantageous aspects of peptide motif molecules are that high stability, interact directly with cell surface receptors, and take up less space on the biomaterial surfaces.[65,66] This allows for additional modifications on the scaffold surfaces. RGD, YIGSR, IKVAV (Ile-Lys-Val-ala-Val) are the most commonly used peptide motif sequences; While RGD molecule is fibronectin-derived, the other ones are laminin-derived molecules.[67] The IKVAV sequence was shown to promote neural cell adhesion, migration, and neurite elongation when used with various biomaterials.[68–72]

Since neural cells are responsible for electrochemical signal transmission, the conductive modifications on the designed biomaterial surfaces can promote neuronal development and differentiation. In addition to conductive polymers that have been used for many years, decoration of scaffold surfaces with gold nanoparticles (AuNPs) has recently aroused great interest. AuNPs are metallic nanoparticles with highly superior physicochemical properties.[73] Based on all these literature data, we aimed to develop channeled PCL/PLGA hybrid scaffolds, modify their surfaces by IKVAV pentapeptide/AuNPs or polypyrrole (PPy) and investigate the behavior of motor neurons on the designed scaffold surfaces in vitro under static/bioreactor conditions. In the in vivo phase of the study, we aimed to investigate the effects of microtopography with ideal channel width, neural factors (BDNF/NGF), and different conductivity approaches (AuNPs or PPy) on the rat spinal cord regeneration. For this purpose, we implanted the designed tubular nerve guidance conduits into the hemisectional spinal cord injury region (T9-T10) of the SD rats and we evaluated the potential of the implant materials to support neural regeneration. Thus, the neural scaffold with the most ideal properties was determined according to the in vitro and in vivo analysis results we obtained.

2. Results

2.1. Characterization of the Prepared PCL/PLGA Film Scaffolds

The main characteristic properties of the synthesized AuNPs were given in **Table 1**.

The seed $AuNP_{20}$ were synthesized by modified Turkevich method and then used for synthesis of medium-sized $AuNP_{50}$ by seeding-growth method. The increase in the size of the AuNPs was confirmed by DLS measurements. It was also confirmed that highly monodisperse nanoparticles were obtained considering the PDI values. Surface plasmon resonance (SPR) peak wavelength changes occurred in the AuNP groups depending on the size. Since all the synthesized AuNPs were citrate-stabilized, their zeta potentials were measured as negative values.

In our previous study, we demonstrated the effect of micro/nano-channeled PCL/PLGA film scaffolds on neuronal differentiation in vitro using the neural stem/progenitor cells.[73] The PCL/PLGA (10:1, v/v) volumetric polymer ratio was evaluated as the suitable group because it had an ideal structure in terms of both flexibility and mechanical strength; Additionally, both polymers are FDA-approved biodegradable biomaterials, and our previous study showed that the degradation profile was suitable for potential neural tissue engineering applications. It was shown that surface modification with IKVAV-pentapeptide and AuNPs made the scaffold surface significantly hydrophilic by reducing the liquid contact angle value.[73] PCL/PLGA (10:1, v/v) film scaffolds produced by spin coating technique with different surface topographies (S and G) and surface modifications (non-conductive and $AuNP_{50}$ coated) were shown in **Figure 1**(A–H). The designed film scaffolds were in the dimensions of 1 × 0.5 × 1, 1 × 5 × 1, 1 × 10 × 1 (ridge × groove × height, μm). We have successfully fabricated PCL/PLGA micro/nano-channeled film scaffolds with the planned topographical features using the Si-wafers we produced with the electron beam lithography technique (Figure 1A–D). The AuNPs generally showed a homogeneous distribution on all the PCL/PLGA film surfaces (Figure 1E–H). The thickness of the PCL/PLGA films was measured as ≈125 microns based on cross-sectional SEM characterization.

FTIR analysis was performed on various films with smooth and fine surfaces in order to detect the functional groups (Figure 1I). The FTIR spectrum demonstrated characteristic and high transmittance peaks at 1721 cm^{-1} that belongs to the conjugated ester group in PCL and at 1746 cm^{-1} that belongs to the free ester group in the PLGA structure.[74,75] The bands that represent symmetrical and asymmetrical $–CH_2$ stretching vibrations of PCL were observed at 2944 cm^{-1} and 2864 cm^{-1}. In addition, –C = O group stretching vibration of the ester bond was detected at 1720 cm^{-1}. The asymmetric stretching vibration band was detected at 1240 cm^{-1}, whereas the symmetrical stretching vibration band was observed at 1160 cm^{-1}. These findings are in accordance with the previous studies.[75] The FTIR spectrum of PLGA showed that the small transmittance band at 3450 cm^{-1} represented –OH stretching vibration and found at the end of the polymer. The C = O stretching vibration peak was detected at 1747 cm^{-1}, while the 1082 cm^{-1} C–O stretching vibration peak represented the primary alcohol group. On the other hand, the stretching vibration band of the ether group was observed at

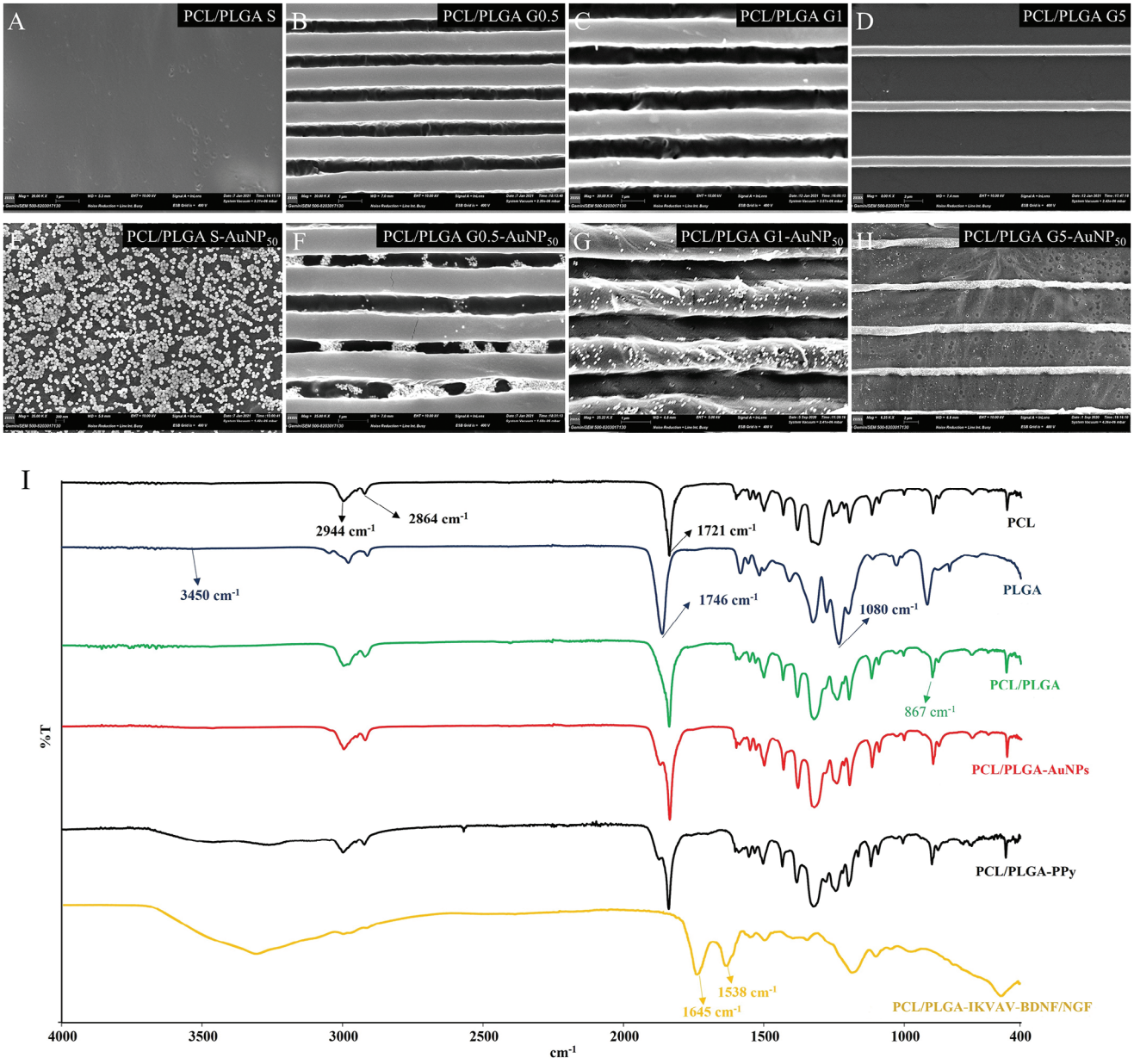

Figure 1. SEM images and FTIR spectra of the designed PCL/PLGA film scaffolds. A) SEM image of the smooth surfaced PCL/PLGA S film scaffold. B–D) Relative SEM images of micro/nano-channeled PCL/PLGA G film scaffolds (500 nm, 1 µm and 5 µm groove widths, respectively). E) SEM image of the smooth surfaced PCL/PLGA S film scaffold decorated with $AuNP_{50}$. F–H) Relative SEM images of micro/nano-channeled PCL/PLGA film scaffold surfaces decorated with $AuNP_{50}$ (500 nm, 1 µm and 5 µm groove widths, respectively). I) FTIR spectra of the designed film scaffolds with various surface chemistries.

1180 cm^{-1}.[76,77] The findings revealed that the FTIR spectrum of the PCL/PLGA (10:1, v/v) was not significantly different since the PCL content in the mixture was higher and the functional groups of PCL and PLGA resembled. The existence of PLGA in the PCL/PLGA mixture was supported by the = C–H stretching peak located at 867 cm^{-1}.[76] The results demonstrated that the peaks of the mixture did not shift and all peaks were available when correlated with individual polymers. This finding showed that the PCL/PLGA mixture did not cause changes in functional groups since it was not newly formed. The coating the surface with AuNPs did not alter typical polymer peaks, which points out that the polymer did not react with Au. In contrast, downward shifts were observed in case of Au surface decorations. The distinctive polypyrrole ring yielded C–N stretching vibrations located at 1554 cm^{-1}, which was observed by the FTIR analysis of PPy coated polymer;[78] Furthermore, the stretching vibration of the N–H bond found in the pyrrole ring caused a wide band at 3195 cm^{-1}.[78,79] In the spectrum coated with BDNF and NGF neurotrophic factors, the characteristic peaks have been detected at the specific Amide I (1645 cm^{-1}, C=O stretching vibrations) and Amide II (1538 cm^{-1} N-H bending and C–N stretching vibrations) regions of the protein structures.

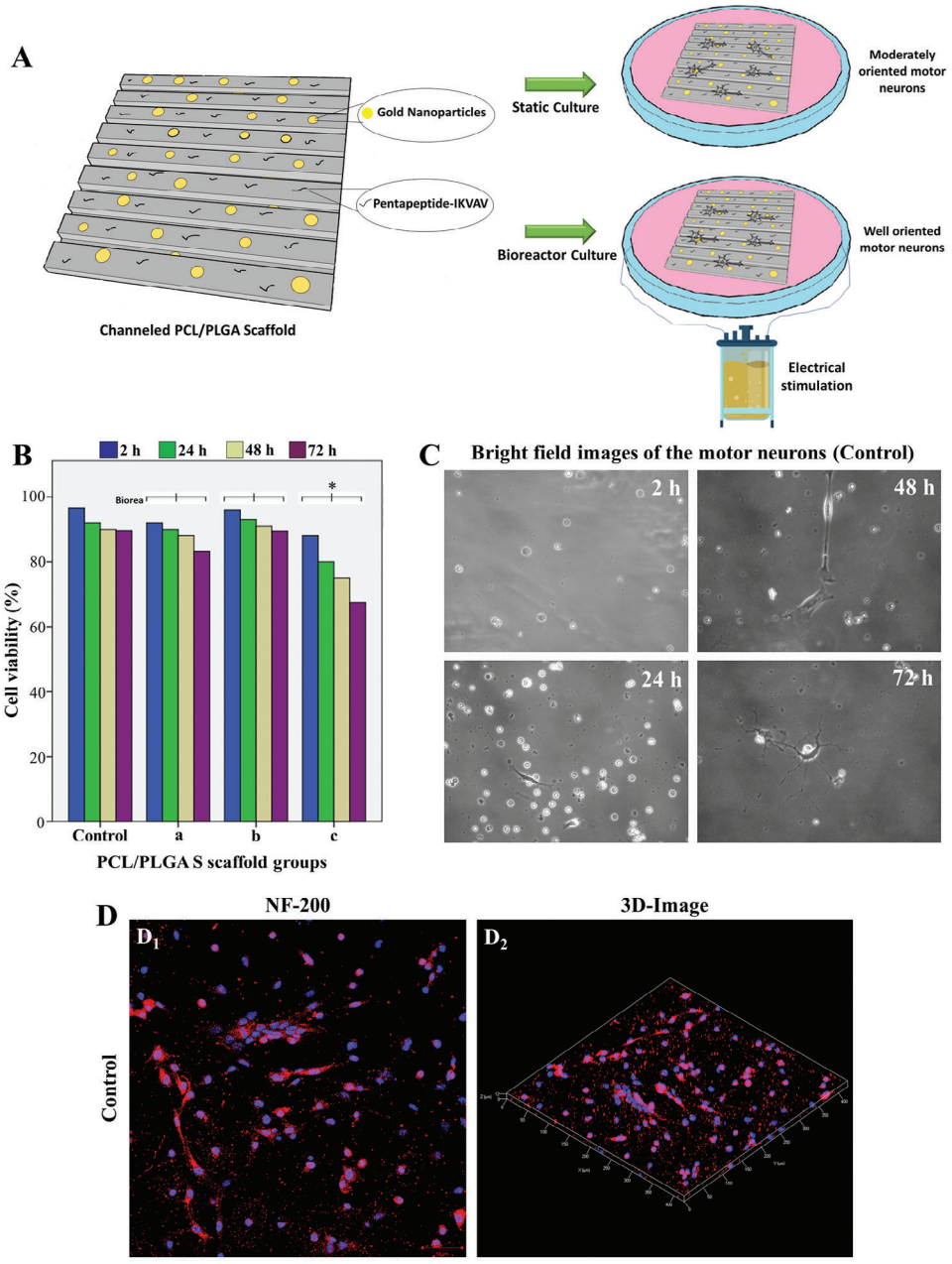

Figure 2. Experimental design, cell viability results and microscopic characteristics of the isolated motor neurons. A) Schematic diagram of the cellular experimental design. B) Cell viability studies of the motor neurons on the various PCL/PLGA S film scaffold groups at different time points. Groups are labeled as; (a) PCL/PLGA S. (b) PCL/PLGA S-AuNP$_{50}$ (c) PCL/PLGA S-PPy. *Different from the control group P<0.05, n = 3, Data were represented as mean ± SD. Data were analyzed by SPSS one-way ANOVA and Tukey post-hoc analysis. C) Bright field images of the motor neurons on the glass-bottomed petri dishes under static conditions for various incubation time points (2 h, 24 h, 48 h, 72 h). (All the images taken by Hoffman modulation contrast microscope, using 20× objective). D) Immunofluorescence LSCM images of the control group (glass-bottomed petri dish) motor neurons showing neural cell skeletons after NF-200 staining incubated on the static conditions for 72 h. (Scale bar = 50 μm).

2.2. The Main Characteristics of the Isolated Motor Neurons and Cytotoxicity of the PCL/PLGA Scaffolds

The in vitro experimental design was shown in **Figure** 2A, before proceeding to the cellular evaluation results. Since the ultimate goal of this study was to evaluate the potential regenerative effects of the designed scaffolds in a spinal cord injury model, the behaviors of the mice spinal cord motor neurons were primarily investigated. Here we show that micro/nano-channeled PCL/PLGA structures with optimal groove sizes can facilitate axonal guidance. We also aimed that the modification of the scaffold surface with PDL/IKVAV-pentapeptide and AuNPs would promote neuronal adhesion and development. In addition, we hypothesized that the axonal guidance of the motor neurons

under the electrical field stimulation can be increased to reach a perfect zero angle guidance with an optimal material design.

Cellular compatibility of the designed smooth surfaced neural scaffold biomaterials with various surface modifications (unmodified, gold nano decorated and PPy modified) was investigated at different hours (2, 24, 48, and 72 h) by using confocal microscope. Figure 2B shows the neural cellular viability (%) results for different PCL/PLGA S film scaffold groups compared to the control group. In the group modified using polypyrrole, which is preferred as the conductive polymer, there was a significant decrease in cell viability compared to the control group. Apart from this, the average neural cellular viability percentages were above 80% in all the other groups over the 3-days period. Thus, no cellular toxicity was observed resulting from the scaffold material itself or AuNPs.

Motor neurons (control group) were incubated for 72 h on the glass-bottomed petri dishes and inverted light microscopy images of the cells were taken on different days (2, 24, 48, and 72 h). (Figure 2C). Neural cellular morphologies were evaluated as generally healthy and no axonal development has yet been observed at 2 h. Axonal development of the motor neurons was clearly observed on other days, and they showed typical motor neuron appearance. Immunocytochemical fluorescence analysis (NF-200 staining) of the motor neurons (control group) cultured in glass-bottomed petri dishes was also carried out before proceeding with cellular studies on the PCL/PLGA film scaffolds (Figure 2D). NF-200 irradiations, which is a neural marker, were strongly taken from both cell bodies and axonal structures, and typically characteristic motor neuron images were observed. Characteristically, motor neurons did not have a highly branched morphology, with the presence of shorter and thicker axonal structures.

2.3. Effect of Micro/Nano-Patterning of PCL/PLGA Scaffolds on Axonal Guidance under Static and Bioreactor Conditions

LSCM images obtained after 72 hours of culture of motor neurons in static conditions show the NF-200 staining results of the cells. Although there were some morphological differences according to PCL/PLGA groups, typically characteristic motor neuron images were observed in general (**Figure 3**); Characteristically, motor neurons did not have a highly branched morphology with relatively thicker axonal structures. There was randomly distributed axonal morphology on all the smooth PCL/PLGA film surfaces and no linear orientation was observed similar to the control group (Figure 3A–C). In general, neuronal structures with unhealthy morphologies and weak axonal developments were observed on all the surfaces coated with PPy due to the possible toxic effect of the polymer (Figure 3C,F,I,L). No unhealthy appearance was observed in the motor neuron cell morphologies on $AuNP_{50}$ decorated PCL/PLGA film surfaces (Figure 3B,E,H,K).

Various levels of axonal orientations were observed along the grooves for the micro/nano-channeled PCL/PLGA scaffold groups (Figure 3G–L). In the groups containing PPy coating, it was observed that neural cellular morphologies were adversely affected and axonal orientation remained at low levels (Figure 3F,I,L).

The cell behaviors of motor neurons cultured on various PCL/PLGA scaffold groups for 3 days under static conditions were quantitatively analyzed. The behavioral analyses were carried out based on LSCM images of NF-200 staining for motor neurons. Quantitative analysis results for axonal orientation behaviors according to different surface topographies and material properties were shown in **Figure 4**A. According to these results, the mean axonal deviations from the channels in the PCL/PLGA G1 group were the least for static culture incubation of the motor neurons (Figure 4A). Again, the deviation level was lower on $AuNP_{50}$ decorated film scaffolds, while it was higher on PPy coated surfaces. So, the optimal axonal guidance was associated with the $AuNP_{50}$ modified micro-channeled PCL/PLGA G1 scaffold having 1×1×1 μm (ridge × groove × height) dimensions and this scaffold group was further evaluated inside the 3D bioreactor system.

Considering the results obtained from static culture studies, the neural film scaffold group with only 1 micron channel width was selected and used in the bioreactor culture studies; Thus, the scaffold material groups with two different surface topographies (smooth-S and 1 μm channeled-G1) and three different surface modifications (unmodified, gold nano decorated and PPy modified) were used in the bioreactor culture studies. Electrical voltage with square wave form was applied in 110 mV mm^{-1}, 1 HZ frequency, and 50 ms pulse for 7 days. It was found that although the electrical stimulation improved the degree of axonal guidance for PCL/PLGA G1 group (non-conductive, Figure 4C,D), perfect approaching zero-degree guidance was seen only on the PCL/PLGA G1-$AuNP_{50}$ scaffolds for both cell types (Figure 4C–E). Again, the axonal morphologies and level of guidance on PPy coated PCL/PLGA G1 scaffolds were not sufficient (Figure 4C–F), similar to the results in the previous static culture conditions.

The mean axonal deviation angles of the motor neurons from the PCL/PLGA channels were shown in Figure 4B for bioreactor system conditions. After electrical stimulation, axonal deviation angles of motor neurons in all the PCL/PLGA G1 groups decreased at a higher rate compared to static culture data. Again, based on the LSCM images of motor neuron cultures in bioreactor conditions, significant axonal guidance approaching zero degrees was observed in the $AuNP_{50}$ modified group. Bioreactor culture data of the motor neurons showed that almost no effect of electrical stimulation for the non-conductive group. On the other hand, as a result of electrical stimulation the axonal deviation angle was significantly reduced for the PPy modified group, it was not at the desired level when compared to the $AuNP_{50}$ group (Figure 4B).

SEM images of the motor neurons cultured under static/bioreactor conditions for 72 hours on the smooth PCL/PLGA surfaces and PCL/PLGA G1 micro-channeled scaffolds, which were considered optimal groove width, are seen in Figure S1 (Supporting Information). According to these SEM images, it can be seen on a high resolution that there was no axonal guidance on all the smooth PCL/PLGA surfaces. (Figure S1 A1–C1, Supporting Information). It has been evaluated that electrical stimulation alone has no effect on axonal guidance of the neurons on the smooth surfaces. Randomly distributed axonal structures were observed on all the PCL/PLGA S surfaces (Figure S1 D1–F1, Supporting Information). Also, it was obvious

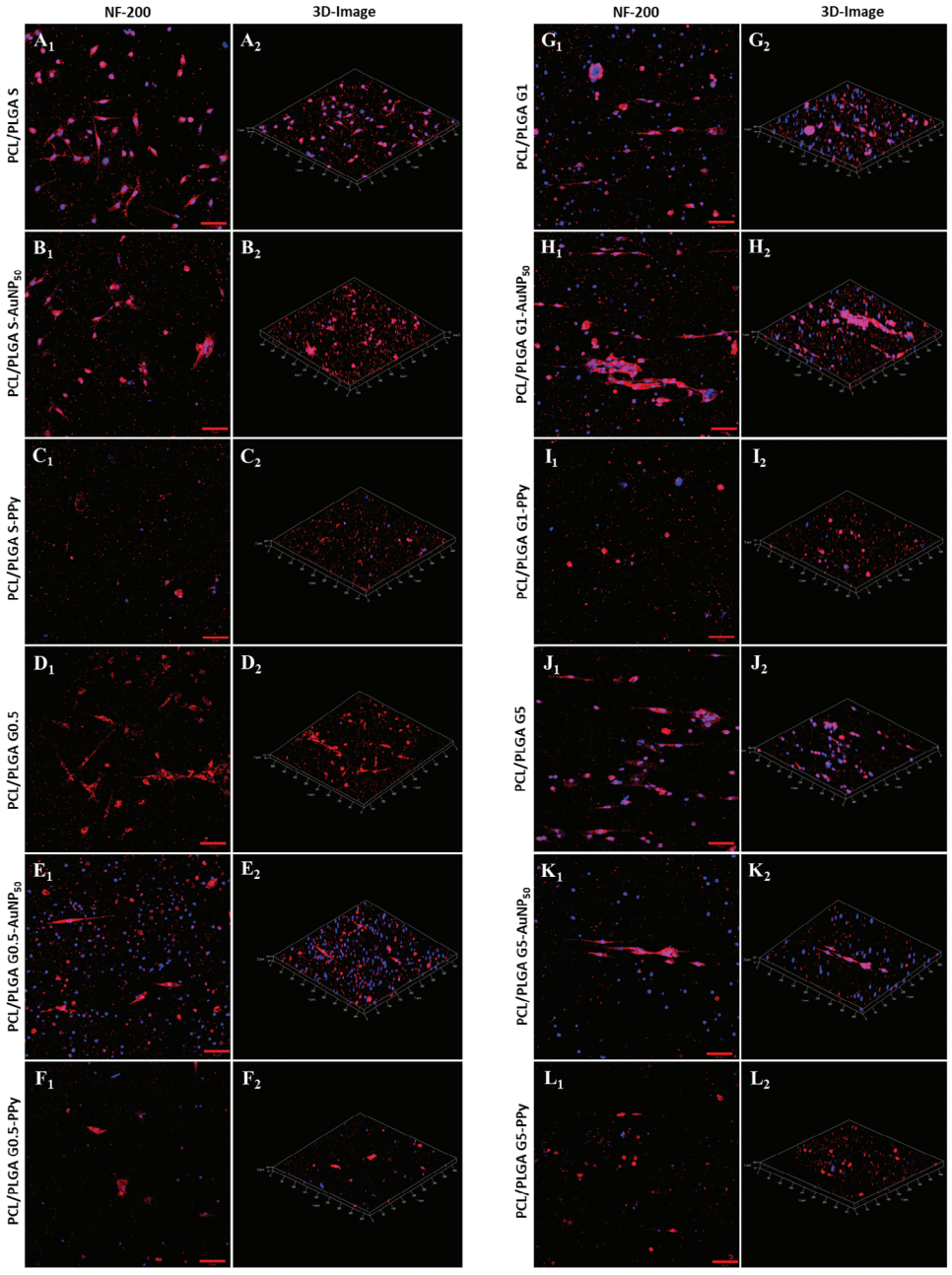

Figure 3. Immunofluorescence LSCM images of the motor neurons showing neural cell skeletons after NF-200 staining incubated on the different PCL/PLGA film scaffolds under static conditions for 72 h. A_1-A_2) PCL/PLGA S. B_1-B_2) PCL/PLGA S-AuNP$_{50}$. C_1-C_2) PCL/PLGA S-PPy. D_1-D_2) PCL/PLGA G0.5. E_1-E_2) PCL/PLGA G0.5-AuNP$_{50}$. F_1-F_2) PCL/PLGA G0.5-PPy. G_1-G_2) PCL/PLGA G1. H_1-H_2) PCL/PLGA G1-AuNP$_{50}$. I_1-I_2) PCL/PLGA G1-PPy. J_1-J_2) PCL/PLGA G5. K_1-K_2) PCL/PLGA G5-AuNP$_{50}$. L_1-L_2) PCL/PLGA G5-PPy. (Scale bar = 50 μm).

that even if there was some degree of axonal guidance on the micro-channeled PCL/PLGA G1 scaffold groups, especially with the effect of electrical stimulation, it was not optimal. (Figure S1 A2,D2, Supporting Information). So, the axonal alignment was better in the AuNP$_{50}$ modified group, consistent with the LSCM images (Figure S1 B2,E2, Supporting Information); Additionally, axonal development and guidance levels were quite insufficient in the PPy-coated group. (Figure S1C2, Supporting Information). Again, the electrical stimulation did not have much positive effect on linear orientation for PPy coated surfaces due to possible toxic effect of the polymer (Figure S1F2, Supporting Information). Above all, it can be seen that under electrical stimulation the degree of guidance was close to zero for AuNP$_{50}$ modified PCL/PLGA G1 scaffold group.

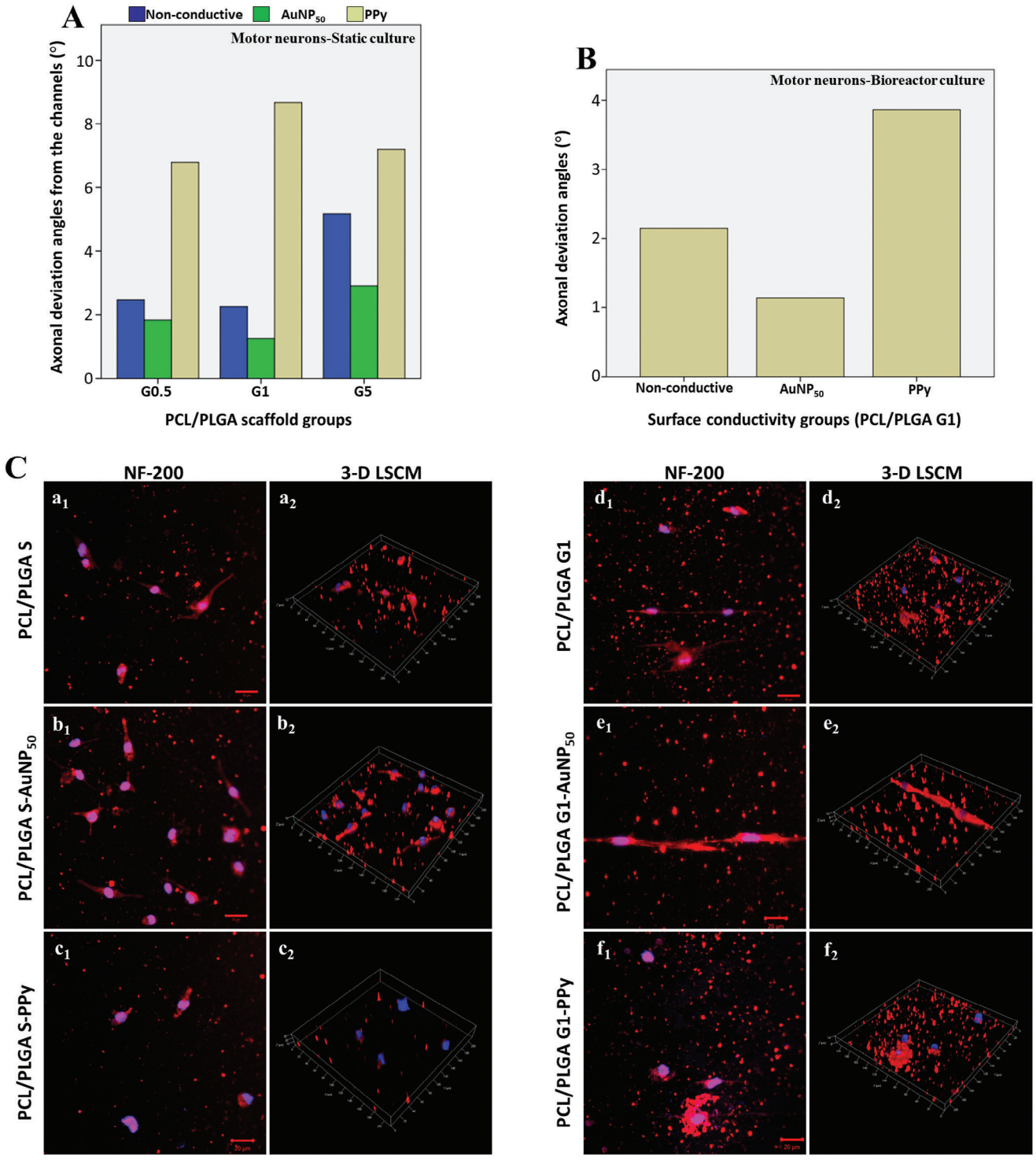

Figure 4. A) The mean values for axonal deviation angles from the micro/nano-channels of the motor neurons cultured on the PCL/PLGA scaffolds with different surface designs under static conditions for 72 h. B) The mean values for axonal deviation angles from the micro-channels of the motor neurons cultured on the PCL/PLGA scaffolds with different surface designs under bioreactor conditions for 72 h. All the quantitative data were obtained using ImageJ program based on the NF-200 (neurofilament-200 kDa) IHC (immunohistochemistry) fluorescence staining images. n = 3, Data were represented as mean ± SD. C) Immunofluorescence LSCM images of the motor neurons showing neural cell skeleton components incubated on different PCL/PLGA film scaffolds under bioreactor conditions for 72 h. (a_1-a_2) PCL/PLGA S. (b_1-b_2) PCL/PLGA S-AuNP$_{50}$. (c_1-c_2) PCL/PLGA S-PPy. (d_1-d_2) PCL/PLGA G1. (e_1-e_2) PCL/PLGA G1-AuNP$_{50}$. (f_1-f_2) PCL/PLGA G1-PPy. (Scale bar = 20 μm).

2.4. Nerve Guidance Conduit Structure and Rat Spinal Cord Injury Model

Schematic diagram of the in vivo experimental design was shown in **Figure** 5A. All the film scaffolds include PDL/IKVAV pentapeptide surface coating as standard. The prepared film scaffolds were wrapped around a microneedle and formed into a tubular shape, then they were fixed with a biocompatible fibrin-based glue. All the tubular PCL/PLGA implant materials were prepared as standard with a length of 3 mm and a diameter of 1 mm (Figure 5B). Back skin was incised by centering the T9-T10 region of the SD rat spinal cord (Figure 5C). Muscle and bone tissues in the midline of the back were successfully incised and removed (Figure 5D). A laminectomy was performed at T9-T10 to allow 3.5 mm right lateral hemisection for NGC implantation by keeping the spine between T8-T11 stable (Figure 5E). After a hemisection lesion of the rat spinal cord, the designed tubular PCL/PLGA nerve guidance scaffold was implanted into the lesion (Figure 5F). After the scaffold transplantation, layer-by-layer suturing was applied (Figure 5G,H shows the dissection images of the spinal cords of the SD rats sacrificed at the 5th and 10th weeks following implantation. With the biodegradability of the implant material and its mechanically flexible structure, a good level of integration was achieved with the spinal cord host tissue, especially at the end of the 10th week.

2.5. Behavioral Recovery

The locomotor recovery was measured by using the BBB in an open field for different weeks (**Figure 6**). The initial score was accepted as "0" for all the experimental groups and each group was compared with the control group in the following weeks. Each week was evaluated separately and the group that achieved significant functional gain compared to the control group was marked with an asterisk in the graph ($P<0.05$); Accordingly, although there is micro-channeled surface topography of the implant, the presence of neural factors and AuNPs increased functional gain, respectively, between weeks 2 and 8. On the other hand, this increase was not statistically significant. The significant functional gain was demonstrated in the group containing only $AuNP_{50}$ surface modification compared to the injured control group at the end of the 10th week. According to these results, although the surface topography of the biomaterial and the presence of neural factors alone contributed positively in terms of functional gain in locomotor scale, the appropriate surface conductivity approach ($AuNP_{50}$) was also an essential parameter for effective nerve regeneration. On the other hand, PPy surface modification of the material led to a negative result in terms of functional gain.

2.6. Histological and Molecular Biological Analysis of Neuronal Regeneration of SCI In Vivo

The immunofluorescence histological analysis and Western blotting studies were performed following implantation of various designed tubular biomaterials into the SD rats at the end of the 5th and 10th week. First, the neural regeneration levels of the different groups were investigated using beta-3-tubulin marker (**Figure 7**). In the control group (injured but not implanted) there was a big gap area at week 5 and no effective regeneration occurred (Figure 7A-a_1). The same result was also valid for the PCL/PLGA S group, still a large non-regenerated gap area was observed for week 5 (Figure 7A-b_1). A prominent injured area was still observed in the groups with micro-channeled topography and modified with neural factors (Figure 7A-c_1,d_1). Considering groups containing conductive surface designs in addition to micro-channeled topography and neural factors, a significantly regenerated area was observed in the $AuNP_{50}$ group compared to the PPy group for week 5 (Figure 7A-e_1,f_1). These LSCM images also overlapped with protein expression analysis results, in general (Figure 7B,C). According to these data, it was observed that micro-channeled topography alone could not provide effective regeneration, but together with neural factors, it made a significant difference. Although the presence of AuNPs provided a high level of beta-3-tubulin expression, the PPy conductivity approach revealed a similar result to the non-conductive group for week 5 (Figure 7C).

When neural regeneration was evaluated at the end of the 10th week following implantation, varying levels of neural regeneration were observed for all groups. Although most of the gap area was regenerated in the injured control group, there were still areas where green fluorescence could not be obtained (Figure 7A-a_2). The results were similar for the PCL/PLGA S group, and an effective neural regeneration could not be achieved (Figure 7A-b_2). In the PCL/PLGA G1 group, nerve fibers were observed extending sequentially in a very thin line (Figure 7A-c_2).

The use of neural factors in combination with micro-channeled topography significantly increased regenerated nerve fibers, although not-regenerated gap regions were present in the peripheral parts for week 10 (Figure 7A-d_2). In the $AuNP_{50}$ modified group, almost completely regenerated spinal cord structure was characterized at the end of the 10th week (Figure 7A-e_2). In contrast, less regenerated nerve fibers were observed in the PPy modified group compared to the non-conductive group (Figure 7A-f_2). Beta-3-tubulin protein expression analysis was also performed for week 10 (Figure 7D,E). There was a proportionally greater increase in neuronal expression (beta-3-tubulin) in all the PCL/PLGA groups modified with neural factors. Micro-channeled topography of the scaffold alone did not provide an effective increase in neural expression. The $AuNP_{50}$ surface modification resulted in a very high level of neural expression, while PPy surface conductivity resulted in lower beta-3-tubulin expression compared to the non-conductive group (Figure 7E).

The astroglial cell development was evaluated by immunofluorescent (GFAP:glial fibrillar acidic protein) histological analysis and Western blotting, after implantation of PCL/PLGA tubular scaffolds into the SC injured area (T9-T10 region) at weeks 5 and 10 (**Figure 8**).

According to the GFAP (glial fibrillar acidic protein) IHC (immunohistochemistry) fluorescence staining results associated with the astroglial scar tissue of the control group (injured), intense irradiations were taken from the defective area, especially at the 5th week, and also GFAP fluorescent irradiations were observed intensively around the injured area at the 10th week (Figure 8A-a_1,a_2). After implantation of the smooth surfaced scaffold (PCL/PLGA S), GFAP irradiations showing astroglial scar

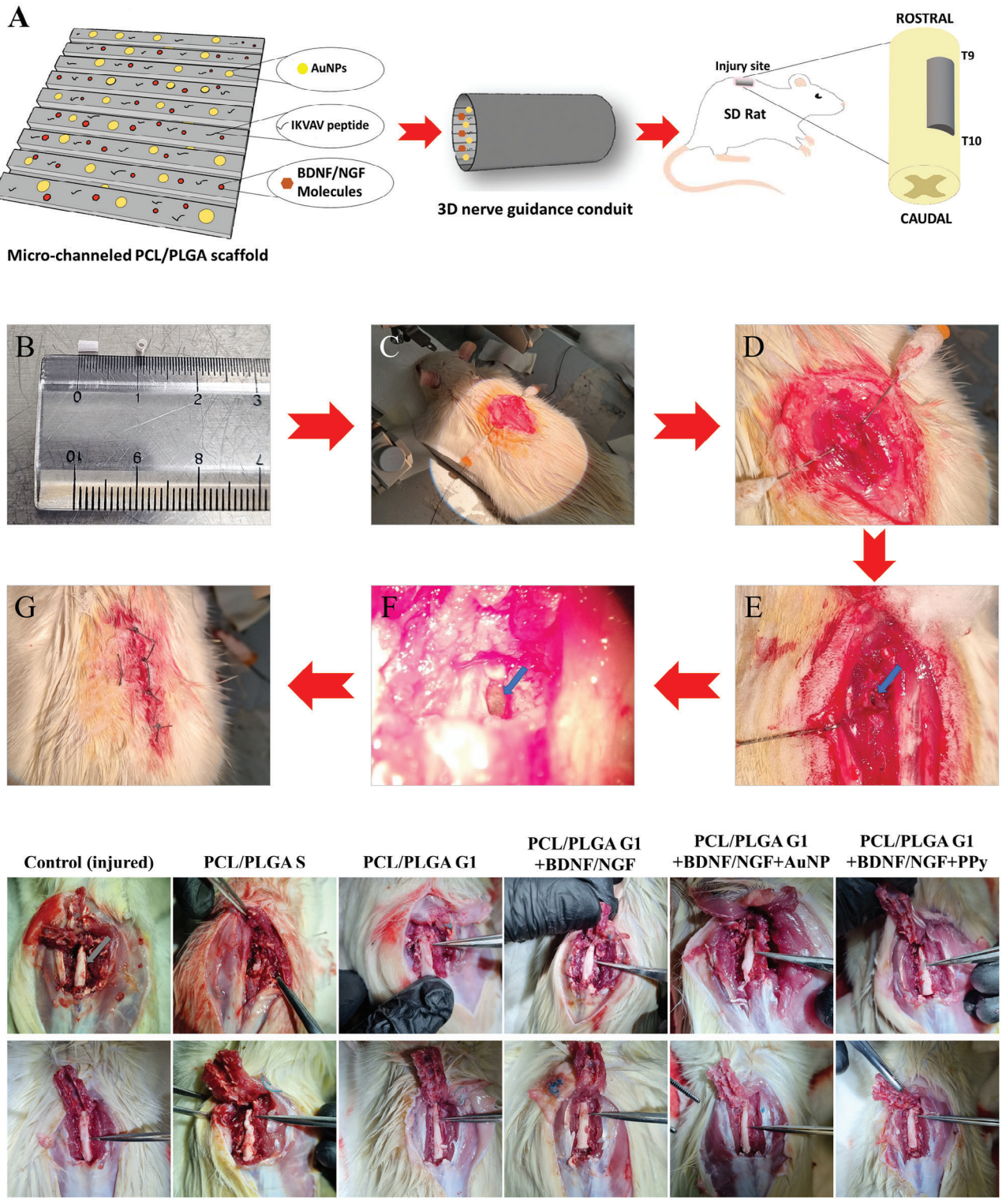

Figure 5. Spinal cord injury model and experimental procedures. A) Schematic diagram of the in vivo experimental design. B) The designed PCL/PLGA tubular implant biomaterial. C) Back skin incised by centering the T9-T10 region of the SD rat spinal cord. D) Muscle and bone tissues in the midline of the back were successfully incised and removed. E) A laminectomy was performed at T9-T10 to allow 3.5 mm right lateral hemisection for NGC implantation by keeping the spine between T8-T11 stable. F) After a hemisection lesion of the rat spinal cord, the designed tubular PCL/PLGA nerve guidance scaffold was implanted into the lesion. G) After the scaffold transplantation, layer-by-layer suturing was applied. H) Dissection images of the spinal cords of the SD rats sacrificed at the 5th and 10th weeks following implantation (the injured area (T9-T10 region) was shown with the forceps tip).

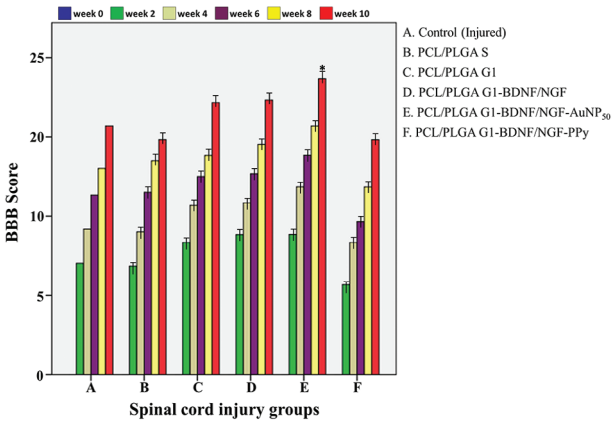

Figure 6. Locomotor recovery was measured by using the BBB in an open field for different weeks. *Different in the direction of increase from the control group P<0.05, n = 3, Data were represented as mean ± SD. Data were analyzed by SPSS one-way ANOVA and Tukey post-hoc analysis. The experimental groups were compared with the control group separately for each week.

tissue formation were especially evident in the injured region similar to the control group at the 5th week. Although GFAP fluorescence decreased in the 10th week, it was still intensely observed around the defective area (Figure 8A-b_1,b_2). According to the GFAP images belonging to the micro-channeled group (PCL/PLGA G1) without any factor or conductivity approach, the intense GFAP irradiations were observed in the 5th week with the secondary injury process. By week 10, GFAP fluorescent images were observed, which showed itself at the borders of the damaged region (Figure 8A-c_1,c_2). The use of micro-channeled PCL/PLGA scaffold topography with the neural factors reduced astroglial fluorescence and minimized GFAP stained SC regions, especially at the end of the 10th week (Figure 8A-d_1,d_2). As a result of surface modification with AUNPs, astroglial fluorescence which was considered as an important barrier to neural regeneration was highly reduced. This data also showed that an effective neural regeneration was achieved (Figure 8A-e_1,e_2). In the PPy-conductive group, very intense astrocyte specific GFAP irradiations were observed around the injured area in week 5. Although GFAP fluorescence decreased by the 10th week, it was still intensely observed around the damaged area (Figure 8A-f_1,f_2). GFAP protein expression was evaluated by Western-blotting analysis as a result of implantation of the various PCL/PLGA tubular scaffolds into the SD rat defective SC cavity (Figure 8B-E). Groups with a significant decrease in GFAP/beta-tubulin protein expression compared to the control (injured) group were indicated by an asterisk. There was a gradual decrease in the GFAP expression according to each parameter change on the PCL/PLGA scaffold surface (smooth surface, micro-channeled topography, neural factors, AuNPs, respectively) for week 5. On the other hand, the PPy conductivity approach led to a similar result to the non-conductive group (Figure 8C). When GFAP expression was evaluated at week 10 post-implantation, interestingly the PCL/PLGA G1 group had a higher GFAP expression rate than the PCL/PLGA S group. The neural factor and $AuNP_{50}$ surface modification of the implant material, respectively significantly reduced the expression of GFAP associated with glial scar formation after secondary injury; However, the PPy surface conductivity approach resulted in higher GFAP protein expression compared to the non-conductive PCL/PLGA group for week 10 (Figure 8E).

Hematoxylin & eosin (H&E) and Masson's trichrome staining were used for general histological analysis of the spinal cords. For this purpose, SD rats under normal maintenance conditions were sacrificed for each experimental group at the end of the 5th and 10th weeks from implantation (**Figure 9**). In the control group (injured), very intense lymphocyte infiltration and axonal degenerations were observed at the injury site for week 5. Also, intense vascularization, fibrotic scar tissue formation and excessive collagen deposition were observed with the inflammatory response developing with secondary injury. In addition to demyelinated and degenerated axonal structures, the cells filled with abnormal brown granules were observed in the peripheral regions (Figure 9A_1,G_1).

When the general histological images of the control group (injured) were evaluated for the 10th week, it was observed that the intense inflammation and scar tissue were replaced by a relatively healthy tissue; However, large non-regenerated regions were still present. The white matter morphology was close to normal and it was observed that the intense collagen deposition decreased which observed for the week 5 (Figure 9A_2,G_2). The general histological images of the group with smooth surfaced, non-conductive, and neural factor-free when evaluated for week 5, very dense fibrous scar tissue formation and excessive collagen deposition were observed in the injured area. Along with the inflammatory response, intense erythrocyte and lymphocyte infiltration occurred, and the excessive bleeding area was noted. In addition, there were intense axonal degenerations in the white matter (Figure 9B_1,H_1). At the 10th week after implantation, very prominent damaged cavities were noted, indicating that an effective neural regeneration could not be achieved. The axonal degeneration was evident and moderately hypertrophic axonal structures were prominent. On the other hand, it was determined that collagen accumulation decreased (Figure 9B_2,H_2). When the images of the group which did not contain any neural factor or conductivity approach and whose surface was 1 µm channeled topography were examined, still unregenerated large gap regions were observed. In addition to fibrous scar tissue formation, intense collagen deposition was observed in the defective area; Additionally, there were significant degenerations in both white matter and gray matter (Figure 9C_1,I_1). Although the injured gap areas were reduced, it was still clearly observed for week 10. Fibrotic scar tissue formation and collagen deposition in the implant region were reduced to minimum levels; However, moderate cellular infiltration and mild axonal disruptions were observed in the white matter (Figure 9C_2,I_2). As a result of the use of neural factors in combination with micro-channeled topography, partially damaged gap regions were evident in the white matter in the 5th week. Fibrous scar tissue formation and collagen deposition were very minimal. Although the gray matter morphology was healthy in general, the axonal distortions were observed in some regions. In addition, cellular infiltration was observed in the white matter (Figure 9D_1,J_1). By the 10th week, it was observed that the spread of the injured gap areas decreased considerably and did not spread throughout the spinal cord tissue. There was no significant collagen deposition in the relevant SC region, and healthy neural cellular structures were observed in both white matter

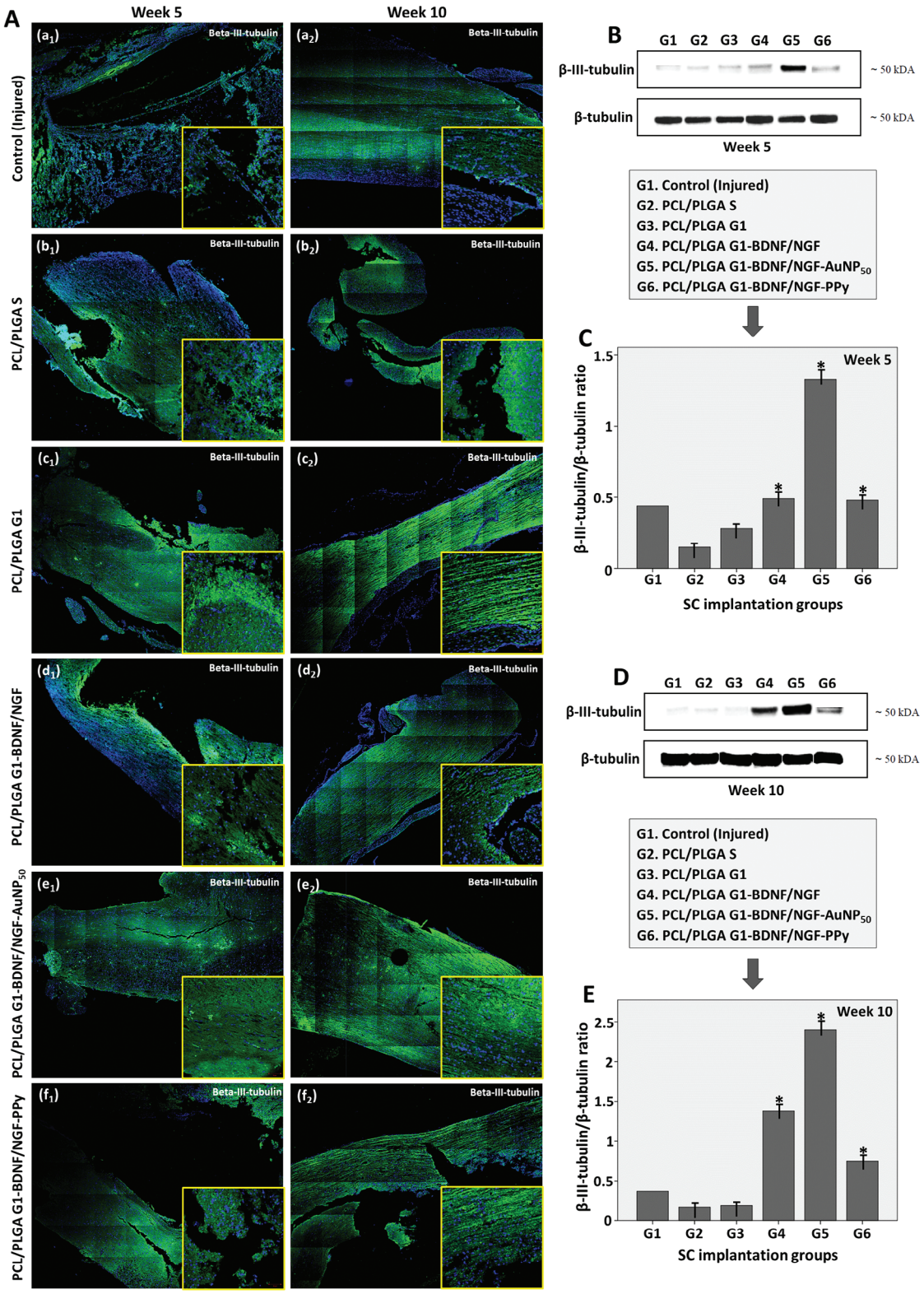

and gray matter (Figure 9D$_2$,J$_2$). In addition to the microtopography of the implant material and neural factor modification, the presence of AuNPs on the PCL/PLGA scaffold surface provided a minimal distribution of damaged cavity regions for week 5; Additionally, minimal levels of fibrotic scar tissue and collagen fiber formations were observed. A low level of cellular infiltration was observed in the white matter, and the axonal structures were healthier than all the other groups (Figure 9E$_1$,K$_1$). It was observed that a very effective level of neuronal regeneration occurred in the AuNP$_{50}$ modified group by the 10th week, and the injured gap SC regions were replaced by healthy neural cellular structures. There were no significant injured SC cavitation areas and the white matter morphology was quite healthy. In addition, fibrous scar tissue formation and collagen deposition were not observed (Figure 9E$_2$,K$_2$). When the general histological images of PPy surface modification group which was another conductivity approach were evaluated, very large, damaged cavities that could not regenerate were observed for week 5. A very intense lymphocyte infiltration with inflammation was observed around the injured SC region and also very prominent axonal degenerations were characterized. In addition, fibrous scar tissue formation and dense collagen accumulations were observed in the area surrounding the damaged SC tissue region (Figure 9F$_1$,L$_1$). In the 10th week after implantation, although the nerve fibers in the regeneration process showed themselves in the injured SC area, large cavity parts were still observed in the related region. The cavitation was evident in the white matter and the cellular infiltration was still present in the gray matter. In addition, reduced levels of fibrotic scar tissue formation and collagen deposition were observed in the gray matter (Figure 9F$_2$,L$_2$).

The LSCM results of other IHC (immunohistochemistry) fluorescence analyses (NF-200 for neurofilaments, CGRP for motor neurons, GAP43 for growth cones, MBP for myelin basic protein, oligodendrocyte, S100-beta for Schwann cells, Iba1 for microglia, CD68 for macrophages) performed in addition to immunofluorescent histological characterizations for beta-3-tubulin and GFAP (glial fibrillar acidic protein) markers were given as supporting information (Figures S2–S5, Supporting Information). These additional fluorescent tissue analyses were performed for each group at 5 and 10 weeks post-implantation. The NF-200 staining results were generally similar to the beta-3-tubulin LSCM data. There were no intense and homogeneous neurofilament-200 irradiations at the desired level for the control group (injured) and PCL/PLGA D group, and there were still non-regenerated gap regions at the end of the 10-week period. Neurofilament irradiations along sequential lines were clearly observed in the micro-channeled groups, and neural factor modification promoted neural regeneration better. Although a very effective neural regeneration was achieved with the contribution of AuNPs, there were still injured gap regions that did not contain neurofilaments in the PPy group at the end of the period (Figure S2A–F, Supporting Information). The CGRP fluorescent radiations specific to motor neurons showed a more homogeneous distribution throughout the relevant spinal cord segment in the groups containing neural factor and AuNP$_{50}$ surface modification. In other groups, it was mostly limited to the SC tissue regions surrounding the damaged area (Figure S2G–L, Supporting Information). The GAP43 marker is associated with the terminal growth cones of nerve fibers in the regeneration process. While GAP43 fluorescence was generally limited to the periphery of the injured area at the end of the first time period, it showed a more homogeneous distribution throughout the spinal cord segment at the end of the 10th week for all the groups; However, the above-mentioned differences were evident between the groups in terms of defective SC gap regions (Figure S3A–F, Supporting Information). The fluorescent irradiations of the myelin basic protein (MBP) were perfectly observed, especially in the AuNP$_{50}$ modified group. This data showed that a functionally effective axonal regeneration occurred for this group (PCL/PLGA G1-BDNF/NGF-AuNP$_{50}$). In other groups, the MBP specific fluorescence was mostly observed in the tissues around the void regions (Figure S3G-L, Supporting Information).

Activation of other glial cells (increase in the number of oligodendrocytes and Schwann cell migration) of the CNS occurs in the secondary injury process after spinal cord damages. The overgrowth of such cells is also a barrier to effective neural regeneration; However, there is a need for the presence of such glial cells in a balanced ratio. According to the IHC fluorescent staining results specific to Oligodendrocyte and Schwann cells, there was a more homogeneous glial cellular distribution throughout the relevant spinal cord segment in groups containing neural growth factor (PCL/PLGA G1-BDNF/NGF) and AuNPs during the 10 weeks period; However, intense glial cellular fluorescent radiations were characterized in the SC tissues surrounding the damaged cavity in the other groups (Figure S4A–L, Supporting Information). Another important pathophysiological aspect of the secondary injury process of spinal cord injury is the migration of defense (immune system) cells. Excessive invasion of these cells leads to a strong inflammatory response. The various chemicals secreted by these cells, and also accumulated oxidative stress ultimately inhibit neural regeneration. For this purpose, IHC fluorescence analyses were performed for microglia cells (Iba1), which are the CNS-specific defense cell type, and macrophages (CD68) migrating to the injured area. According to LSCM results, very intense microglial activation was observed in the control group (injured) and smooth surfaced implant group

Figure 7. Neural regenerative effects of the various PCL/PLGA nerve guidance conduit designs obtained from histological analysis and Western blotting after a hemisection lesion of the rat spinal cord for two different weeks (week 5 and week 10). A) Immunofluorescence LSCM images of the rat spinal cord paraffin sections in the longitudinal direction showing neuronal axons after beta-III-tubulin staining (green fluorescence) for various implantation groups. (a_1-a_2) Control (Injured). (b_2-b_2) PCL/PLGA S. (c_1-c_2) PCL/PLGA G1. (d_1-d_2) PCL/PLGA G1-BDNF/NGF. (e_1-e_2) PCL/PLGA G1-BDNF/NGF-AuNP$_{50}$. (f_1-f_2) PCL/PLGA G1-BDNF/NGF-PPy. Representative LSCM images of the middle and the boundaries (rostral and caudal ends) of the injured area. All the images taken by using 20× objective. The main images represent the tile-scan mode imaging, the small squares represent the normal mode images, and the blue radiations are the DAPI cell nuclei staining. B,C) Western blot analysis of beta-III-tubulin expression in the rat spinal cord after injury for week 5 (n = 3 for each group). D,E) Western blot analysis of beta-III-tubulin expression in the rat spinal cord after injury for week 10 (n = 3 for each group). The representative results of Western blot were shown in the upper panel, and the statistical analysis was shown in the lower panel. β-tubulin was used for the quantitative normalization. *Different in the direction of increase from the control group, P<0.05. Data were represented as mean ± SD. Data were analyzed by SPSS one-way ANOVA and Tukey post-hoc analysis.

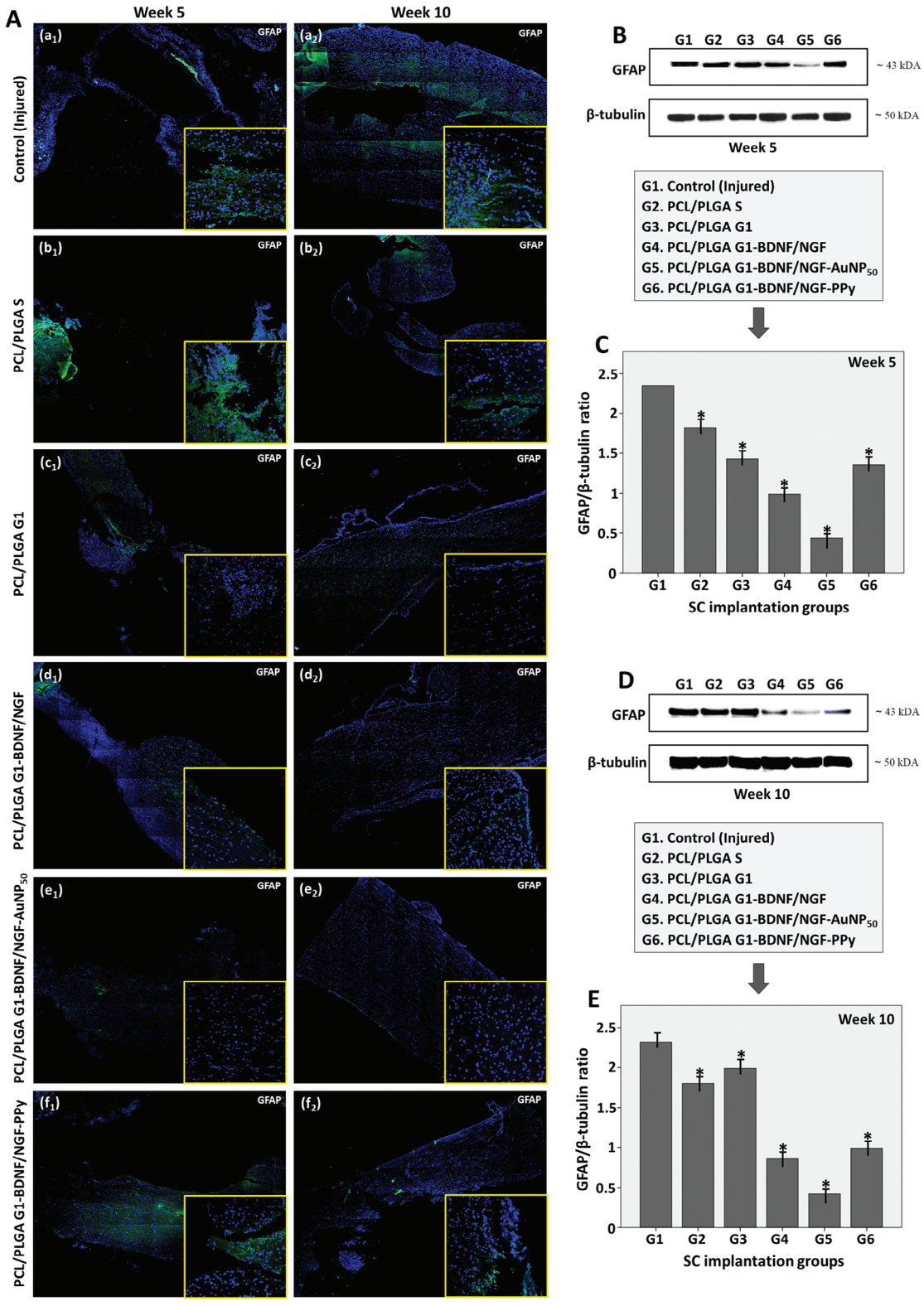

(PCL/PLGA S) in week 5. Although it decreased in week 10, it was still intense around the damaged area. Among the micro-channeled groups, the most ideal results were obtained from the groups containing the neural factor (PCL/PLGA G1-BDNF/NGF) and the $AuNP_{50}$ surface modification. As a result of insufficient neural regeneration in the damaged spinal cord region for the other groups, the inflammatory response and the existence of such defense cells continued. The inflammatory response was reduced because the ideal group (PCL/PLGA G1-BDNF/NGF-$AuNP_{50}$) promoted neural regeneration at a high level as a result of the triple synergistic effect (high level orientation of the axons of the neurons on the micro-channeled surface, promotion of the regeneration by neural factors, suitable surface conditions provided by conductive AuNPs) of the implant material. In the other groups, microglial activation was still present at the end of the 10-week period, although decreased (Figure S5A–F, Supporting Information). LSCM images of macrophage migration were also consistent with microglial data. These results about macrophage cell migration confirmed that the presence of neural factors and AuNPs combined with the micro-channeled material topography reduced inflammation (Figure S5G–L, Supporting Information).

3. Discussion

Spinal cord injuries (SCI) occur tragically in the people under the age of 30 who are the youngest and most active segment of the society with a frequency of 60%, and their pathophysiology is considered in two separate categories as primary and secondary phase. The primary injury after a concussive trauma mainly damages the gray matter, leading to bleeding and impaired blood flow. On the other hand, secondary injury refers to the spread of injury from the first part to the adjacent tissues as a result of various response reactions, and it manifests itself with various pathophysiological events (such as ischemia, thrombosis, hypoxia, oxidative stress, oxidation, disruption of membrane integrity, edema, protein degradation, apoptosis, necrosis, disruption of synaptic connections, demyelination, axonal degeneration).[80–83] There are two options for treatment after spinal cord injury: neuroprotection (preventing the spread of secondary damage) and regeneration. Neuroprotective treatments can be administered with drugs (such as methylprednisolone sodium succinate, immunoglobulin G, granulocyte colony-stimulating factor, minocycline, riluzole) or non-pharmacological strategies (such as systemic hypothermia).[84–89] The aim of regeneration is to restore neuronal transmission and functional gain. While SC regeneration can be achieved using various pharmacological therapies (such as anti-Nogo-A antibody, Rho-ROCK inhibitor, anti-RGMa-antibody), effective functional recovery can also be achieved with cellular and novel biomaterial-based approaches.[84,90–92] The other ones are cell-based and stem cell-based treatments, which are considered approaches to promote functional recovery. On the other hand, there are still design challenges in terms of clinical effectiveness, such as low effect sizes, low sensitivity, and insufficient immunosuppression. The difficulties and limiting factors in the cell-based therapies have paved the way for innovative integrated therapies including various biomaterials. Especially, gene regulation, cell sequencing and tracking have emerged as promising avenues of investigation.[93] The development of innovative treatment methods and in-depth study of the SCI microenvironment has become possible by current technology.[94] The sequential progression of axons and neurites along a linear line is extremely important for effective regeneration and functional recovery after a nerve injury.[95] Scaffold-based strategies have recently attracted great interest to counteract the trauma environment after SCI by providing a supportive structure to damaged neurons and tissues. Apart from providing support, there are also many studies in which other components (different cells, factors, enzymes, conductive materials, etc.) that promote the survival, differentiation of neural cells and the guidance of damaged axons are included in the structure.[96–98] Neuroinflammation and glial scar formation in the damaged SC area is an important factor that inhibits the migration, differentiation, and regeneration of neural cells. In the literature, some studies using various hydrogels and nanoparticles after SCI have shown that inflammation/glial scar tissue formation was reduced and significant functional gains and neural regeneration were achieved.[99–105]

The ideal scaffold for neural regeneration must provide a 3D interconnected porous structure and suitable physicochemical properties, such as mechanical strength, elasticity, stiffness, hydrophilicity, and surface conductivity. The designed scaffold should display an ideal biocompatibility profile and suitable degradation rate over time. In addition, the use of neural tissue scaffolds in combination with neurotrophic factors is another parameter that will promote nerve regeneration. Synthetic polymeric biomaterials that are developed according to controlled degradation rates and physicochemical properties have many advantages in terms of neural implant biomaterial fabrication. In addition, they can be designed as mechanically strong, elastic, hydrophilic, and biocompatible with controlled fabrication techniques and surface modifications.[17,73,95] While the PCL material used in this study provided mechanical strength, PLGA supplied flexibility to the hybrid polymeric scaffold. The PCL/PLGA (10:1, v/v) volumetric ratio was evaluated as suitable and all the cellular and in vivo studies were carried out by this optimal polymeric ratio. Our previous study showed that the degradation profile was suitable for neural tissue engineering applications. It has been

Figure 8. Astroglial scar development effects of the various PCL/PLGA nerve guidance conduit designs obtained from histological analysis and Western blotting after a hemisection lesion of the rat spinal cord for two different weeks (week 5 and week 10). A) Immunofluorescence LSCM images of the rat spinal cord paraffin sections in the longitudinal direction showing astrocytes after GFAP (glial fibrillar acidic protein) staining (green fluorescence) for various implantation groups. (a_1-a_2) Control (Injured). (b_2-b_2) PCL/PLGA S. (c_1-c_2) PCL/PLGA G1. (d_1-d_2) PCL/PLGA G1-BDNF/NGF. (e_1-e_2) PCL/PLGA G1-BDNF/NGF-$AuNP_{50}$. (f_1-f_2) PCL/PLGA G1-BDNF/NGF-PPy. Representative LSCM images of the middle and the boundaries (rostral and caudal ends) of the injured area. All the images taken by using 20× objective. The main images represent the tile-scan mode imaging, the small squares represent the normal mode images, and the blue radiations are the DAPI cell nuclei staining. B,C) Western blot analysis of GFAP expression in the rat spinal cord after injury for week 5 (n = 3 for each group). D,E) Western blot analysis of GFAP expression in the rat spinal cord after injury for week 10 (n = 3 for each group). The representative results of Western blot were shown in the upper panel, and the statistical analysis was shown in the lower panel. β-tubulin was used for the quantitative normalization. *Different in the direction of decrease from the control group, $P<0.05$. Data were represented as mean ± SD. Data were analyzed by SPSS one-way ANOVA and Tukey post-hoc analysis.

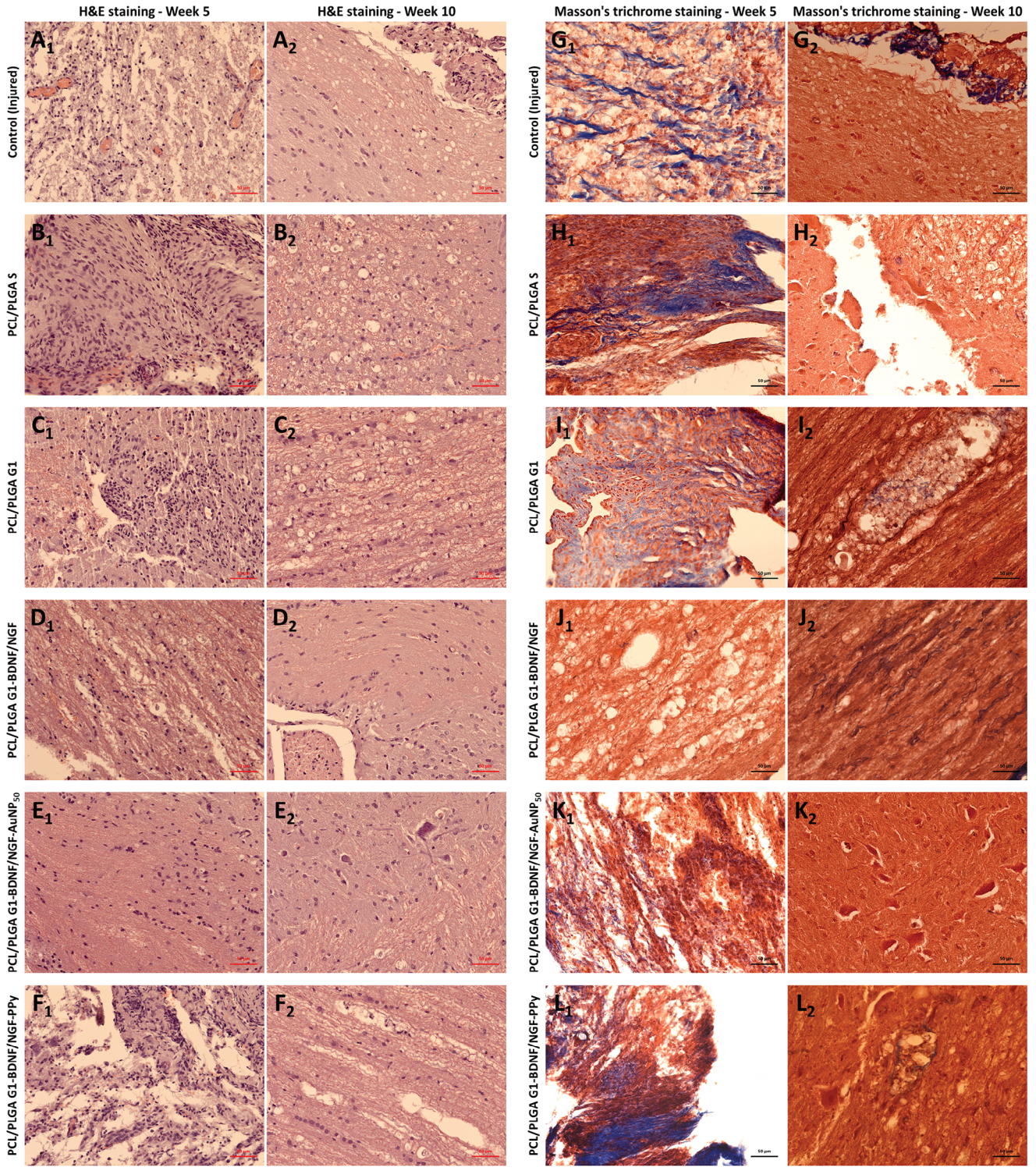

Figure 9. General histology evaluations of the various PCL/PLGA tubular scaffolds on the microstructural changes in the spinal cord injury region of SD rats for the 5th and 10th weeks following implantation. A–F) Hematoxylin & eosin (H&E) staining images. G–L) Masson's trichrome staining images. All the images taken by using 20× objective. (Scale bar = 50 µm). A,G) Control (injured). B,H) PCL/PLGA S. C,I) PCL/PLGA G1. D,J) PCL/PLGA G1-BDNF/NGF. E,K) PCL/PLGA G1-BDNF/NGF-AuNP$_{50}$. F,L) PCL/PLGA G1-BDNF/NGF-PPy.

shown that surface modification with IKVAV-pentapeptide and $AuNP_{50}$ made the scaffold surface significantly hydrophilic by reducing the liquid contact angle value.[73]

Using Si-molds designed with electron beam lithography technique, micro/nano-channeled PCL/PLGA film scaffolds with three different groove widths were fabricated successfully. Patterned PCL/PLGA film scaffolds with 1 µm channel width gave the most promising results under static culture conditions (no electrical stimulation) in our in vitro study. In various studies in the literature for neural tissue engineering, in which films and scaffolds with periodically parallel micro/nano channel structure were used, sometimes it was seen that lithographic patterns were applied directly to the substrate polymer itself,[47,106,107] and sometimes it was applied to the biomaterials to be used as a mold.[108–111] Yang et al showed that functional neuron expression and neurite alignment increased when the human neural stem cells were cultured on hierarchically patterned topographies (with 10 nm nanopores and 1.5 µm channel width).[111] Slightly different, in a study using human induced pluripotent stem cells, Pan et al observed that neural expression and linear orientation were highest in the group with 350 nm groove width when cells were incubated on the PDMS substrates with different groove widths (350 nm, 2 µm, and 5 µm).[109] In two different studies, it has been shown that the neurite elongation and neural cellular development were higher on the surfaces with a groove width of 1 µm similar to our finding.[112,113] These results reveal that optimal channel/groove widths may vary according to neural cell type. Especially, since the motor neurons we used in this study are the cells with a relatively large diameter and axons. In our study, PCL/PLGA film scaffolds with 1 µm channel width provided the optimal condition for effective axonal guidance. The $AuNP_{50}$ nano-decoration used to provide a conductivity on the micro/nano-channels did not cause any adverse effects on the motor neurons. On the other hand, adverse effects of PPy on the neural cells were observed in both cellular viability studies and LSCM/SEM analysis results. Within the scope of bioreactor system studies, it was observed that although the electrical stimulation improved the degree of axonal guidance for PCL/PLGA G1 group, perfect approaching zero-degree guidance was seen only on PCL/PLGA G1-$AuNP_{50}$ scaffold group. Conductive polymers, also called electroactive polymers are a series of polymer materials that allow the transfer of electrical stimuli to neural cells.[114] It has been evaluated that the surface conductivity approach provided by AuNPs can be a good alternative to the conductive polymer that has been used for many years.

PCL and PLGA, both as FDA-approved biocompatible polymers, have been frequently preferred in the literature for in vivo studies within the scope of tissue engineering. In an in vivo study, implantation of the microporous multi-channeled PCL tubular scaffold into a complete-section rat SCI model (T3 region) were investigated. It has been shown that implantation of the designed biomaterial into the defective region supported minimal glial scar tissue formation and also promoted linear axon elongation.[115] Silva et al. designed a 3D scaffold based on a mixture of PCL and starch. They showed that the stabilization of the spinal cord architecture was increased with the bone-adjacent scaffolds and the gain of motor function improved at week 12 following implantation into the rat spinal cord injury.[116] In the literature, PLGA (alone or hybrid polymer forms) has been implanted into the SCI models (rats or mice) in different structures such as nanofibrous micro-channeled scaffold, tubular multi-channeled scaffold, and 3D nanofibrous scaffold for the regeneration of spinal cord injury. In these studies, a good integration with neural tissue and low level of immune response were observed after implantation. In addition, it has been shown that the significant axonal regeneration was achieved, and the neurite guidance and density were increased.[50,51,117,118] In this study, comprehensive evaluations were made as a result of the implantation of various tubular PCL/PLGA scaffolds into the rat spinal cord hemisection injured area (T9-T10 region). In addition to the inner surface topography of the conduit material, the potential effects of the neurotrophic factors (BDNF/NGF) and two different surface conductivity approaches ($AuNP_{50}$ and PPy) on the spinal cord regeneration were revealed with analyses performed at the 5th and 10th weeks after implantation. All the histological and molecular biological analysis results showed that the surface topography (micro-channeled surface) of the biomaterial to be implanted alone cannot provide an ideal result for an effective neural regeneration. Implant biomaterials with surface topography that can guide axons will provide more effective and functional neural regeneration when used in combination with neural factors and optimal conductivity approach. We show that the developed optimal nerve guidance conduit (PCL/PLGA G1-IKVAV/BDNF/NGF-$AuNP_{50}$) highly regenerates spinal cord injury. It was also evaluated that the glial scar tissue development was minimized and functional recovery was successfully achieved in this optimal group. Similar to in vitro results, effective neural regeneration could not be achieved in the groups with smooth surfaced and PPy conductivity modification. In addition, inflammation caused by the invasion of the immune cells/glial cells and the collagen deposition associated with glial scar tissue formation were high levels in these groups. This can be explained by the possible toxic effect of PPy and its inability to create a suitable surface chemistry for the development of neural cells. AuNPs promoted axonal guidance as they accumulated mostly along grooves without forming large aggregates, creating conductive nanoarrays on the scaffold surface. Additionally, it was evaluated as an advantageous group with its biocompatibility and physicochemical properties that would support neuronal development and cell adhesion.

The synergistic effects of BDNF and NGF also significantly increased the level of SC regeneration, in addition to the advantages provided by AuNPs and microtopography. In the central nervous system, NGF molecule has neuroprotective effects and can influence neural responses to injury on the various neural cell types that display NGF receptors. Binding of NGF molecule to TrkA and p75-NTR receptors activates downstream signaling pathways such as MAPK/ERK, PI3K/Akt and PLC-γ. As a result of this signaling mechanism, the survival and differentiation of the neural cells is promoted.[119] BDNF molecule has neuroprotective and growth-promoting effects on the different neural cell types after nerve injury. In the literature, the neuroprotective properties of BDNF are explained by the downstream effects of the TrkB receptor signaling pathway. TrkB is expressed abundantly in the neurons of the spinal cord and these neurons can also undergo upregulation of TrkB receptors during SC injury.[120] In a study, the neuroprotective effect of BDNF molecule on the corticospinal neurons was demonstrated after grafting of BDNF-secreting mesenchymal stem cells to the T9 spinal cord injury

area compared to the lesioned control group.[121] In another study, the linear ordered collagen scaffold-BDNF complex has been shown to significantly promoted functional recovery after completely transected spinal cord injury in the canine model.[122] Taken together, positive effects of the neurotrophic factors make them promising candidates for a future SCI treatment. The use of neurotrophic factors in combination with treatments that help improve lesion environments, such as polymeric scaffolds or nerve guidance bridges, has the potential to promote meaningful functional regeneration after spinal cord injury.

4. Conclusion

In this study a functional channeled and $AuNP_{50}$ conductive PCL/PLGA tubular nerve guidance conduit with modified BDNF/NGF/IKVAV pentapeptide molecules has been developed for regeneration of the rat spinal cord injury in long-term period. We show that channeled scaffold groups decorated with AuNPs highly promote neurite orientation under bioreactor conditions and also the developed optimal nerve guidance conduit (PCL/PLGA G1-IKVAV/BDNF/NGF-$AuNP_{50}$) highly regenerates spinal cord injury. The synergistic effects of BDNF and NGF also significantly increased the level of SC regeneration, in addition to the advantages provided by AuNPs and microtopography. Our micro/nano-designed PCL/PLGA scaffolds can be used as nerve conduits in nerve tissue engineering to provide optimal axonal guidance and neural regeneration required for recovery of function after various nerve injuries.

5. Experimental Section

Gold Nanoparticle Synthesis and Characterization: The use of the gold nanoparticles ($AuNP_{50}$) on the PCL/PLGA film scaffolds within the scope of neural tissue engineering was demonstrated previously.[73] First, seed gold nanoparticles ($AuNP_{20}$) were synthesized by a modified Turkevich synthesis method[123] and then used for synthesis of the 50 nm diameter gold nanoparticles ($AuNP_{50}$) by seeding growth method.[124] The synthesis was carried out according to the previously reported protocols.[125] In the first stage, trisodium citrate dihydrate (reducing agent, Sigma-Aldrich) was added to the boiling 0.25 mM chloroauric acid ($H[AuCl_4]$, Sigma-Aldrich) solution at a concentration of 0.033%. Synthesized AuNPs were washed by centrifuging (Thermo-Scientific, MicroCL 21R) at 7 000 g for 30 min and redispersed in ultrapure water. In the second stage (the seeding growth protocol), the synthesized seed particles, reducing agent, and hydroquinone (Sigma-Aldrich) were added in the required concentrations to 100 ml of 0.25 mM gold solution at room temperature. After centrifugation and redispersion in the ultrapure water, the necessary characterization procedures (DLS-Malvern and UV–Vis absorption spectroscopy-Shimadzu) were carried out. The Au concentration in the synthesized AuNPs samples was precisely confirmed by ICP-MS (PerkinElmer) measurements.[73,125]

Preparation and Characterization of the Micro/Nano-Channeled PCL/PLGA Film Scaffolds: In order to prepare the micro/nano-channeled PCL/PLGA film scaffolds, silicon wafer molds (1 × 1 cm^2; 0.5, 1, 5 µm ridge widths; 1 µm channel width; 1 µm channel height) were prepared by standard e-beam lithography technique, as described in the previous work.[73] Briefly, after dissolving PCL (3% w/v, Sigma, 80 000) and PLGA (5% w/v, Sigma, 66000–107000) separately in chloroform, they were volumetrically mixed (10:1 v/v) to obtain hybrid polymer solution. Using the spin coating technique, smooth surfaced and channeled PCL/PLGA film scaffolds with various groove widths (500 nm, 1 µm and 5 µm widths) were obtained. Sterilization of the biomaterials obtained was achieved with 70% ethanol (Sigma) and short-term UV exposure for cell culture studies. Two different surface modifications ($AuNP_{50}$ and PPy) applied to obtain various surface conductivity designs, in addition to the surface topography. For this purpose, 200 µl of $AuNP_{50}$ stock solution (50 µg Au/ml) was directly added to scaffolds and dried overnight. Alternatively, the surfaces of the scaffolds were coated to form a thin layer using polypyrrole (PPy, 5 wt.% dispersion in H_2O, 1:500 dilution, Sigma-Aldrich). All the surface modification processes were carried out in the laminar flow cabin under sterile conditions (Thermo Maxisafe 2020 Class II). Non-conductive materials were also used to compare with conductive surfaces in the cell culture studies. All the prepared scaffolds were characterized by SEM (Zeiss Geminisem 500). The biomolecule surface coatings were applied on the prepared film scaffolds before the neural cellular studies. First, poly-D-lysine (PDL, 10% v/v, Sigma-Aldrich) surface modification was applied to form a very thin layer on the materials and dried under sterile conditions. Second, the film scaffolds were coated with IKVAV-pentapeptide (Ile-Lys-Val-ala-Val) solution (0.2 mg mL^{-1}) to form a very thin layer on the material surface and dried. For in vivo studies, the film scaffolds were additionally modified with NGF and BDNF (100 µg mL^{-1}, Sigma-Aldrich) to form a thin and homogeneous layer over the entire surfaces. Fourier transform infrared spectroscopy (FTIR, Pelkin Elmer) was used to identify functional groups found on the prepared film scaffold according to various surface modifications (PDL/IKVAV/NGF/BDNF, $AuNP_{50}$ and PPy).

Isolation and Culture of the Motor Neurons: All the animal procedures were performed under Istanbul Medipol University, Institutional Animal Care and Use Committee (IMU-HADYEK). Younger mice were used instead of adult mice for the isolation of motor neurons. For this purpose, 40 BALB/c mice (20 female and 20 male) were used. Following anesthetization with Ketamin (Pfizer, 100 mg $k^{-1}g$, IP) the mice were decapitalized. The posterior surface of the vertebral column, which was parallel to the ground was removed from the cervical to the lumbar on a cold steel table. The spinal cord exposed by removal of the bone structure was washed in half-frozen L15 medium (containing; 2% B-27 supplement-Gibco, 1% antibiotic/antimycotic-Sigma-Aldrich and 1% glutaMAX-Gibco). A piece of spinal cord, ≈1–2 cm long and containing the anterior horns, was placed in NBA (Gibco) culture medium (containing 2% papain enzyme, Sigma-Aldrich) and incubated at +4 ^{0}C in a shaker setup for 30 min. Mechanical separation was achieved by trituration using pipette tips of varying diameters. After incubating with DNase (50 mg mL, Sigma-Aldrich) solution, the neural cells were centrifuged at 120 g for 3 min and the cell pellet was dispersed in NBA culture medium. The obtained motor neuron cell suspension was seeded on 10% (v/v) PDL and 1% (v/v) IKVAV-pentapeptide pre-coated petri dishes (250 cells/petri). Neural cells incubated (95% air, 37 °C, 5% CO_2, 21% O_2) for 3 days and inverted light microscopy images of the motor neurons were taken at different time points (2, 24, 48, and 72 h). (Zeiss-Hoffman Modulation Microscope).

Cytocompatibility Evaluation of the Prepared PCL/PLGA Scaffolds: All the prepared smooth PCL/PLGA film scaffolds (PCL/PLGA S, modified/unmodified) were sterilized by using 70% alcohol and UV irradiation (30 min). The sterile film scaffolds were placed in glass-bottomed petri dishes and each of the neural cells were seeded individually on the scaffolds (250 cells/scaffold for motor neurons) and cultured in NBA culture medium under the optimum culture condition (37 °C, 95% air, 5% CO_2, and 21% O_2) for 72 h. PDL and IKVAV coated glass petri dishes were used as a control group. Propidium iodide (PI, Thermo Fisher-Invitrogen) staining was carried out and percent cell viability was evaluated under the laser scanning confocal microscope (LSCM, Zeiss LSM 780) in 2 h, 24 h, 48 h, and 72 h time intervals. The nucleus of the dead cells was stained red with PI staining so under the T-PMT mode of the microscope and using 20× objective 10 random areas were selected and after counting the dead cells, average dead cell numbers were used to calculate the percent cell viability by the following equation.[126]

$$\text{Cell Viability (\%)} = (\text{Total cell count} - \text{Dead cell count}) / (\text{Total cell count}) \times 100 \quad (1)$$

Statistical analysis was performed by using SPSS Statistics 22 software and One-way analysis of variance (ANOVA-Tukey post-hoc analysis) was performed to determine inter-group differences ($p < 0.05$). $n = 3$, Data were represented as mean ± SD.

Motor Neuron Culture Studies on the PCL/PLGA Film Scaffolds under Static/Bioreactor Conditions: In order to evaluate the effects of the engineered micro/nano-channels on neural cellular behaviors under static (no electrical stimulation) and bioreactor conditions (with electrical stimulation), isolated motor neurons were cultured on the prepared PCL/PLGA film scaffolds. It had also evaluated the effects of different chemical surface modifications (non-conductive, $AuNP_{50}$ coated, PPy modified) on the neural cell behaviors with the in vitro studies, in addition to topography. Motor neurons were seeded on the scaffolds (250 cells/cm^2 for motor neurons) and were cultured for 72 h in NBA culture medium (1% antibiotic, 1% glutamax, and 2% B27) under optimal culture condition (37 °C, 95% air, 5% CO_2 and 21% O_2). Within the scope of bioreactor culture studies, electrical stimulation was applied to the motor neurons, using a computerized bioreactor system (EBERS Medical Technology SL). Three various surface conductivity groups (non-conductive, $AuNP_{50}$ modified, PPy modified) and two various surface topographies (S and G1-optimal groove width) were used for the bioreactor culture studies. The neural cellular studies within the scope of the bioreactor system were carried out over a 72-h period as previously described.[73]

Immunofluorescence Staining and LSCM Characterization of the Motor Neurons: Immunocytochemical fluorescence analysis of the cultured motor neurons (for static and bioreactor culture conditions) was performed for 72 h to determine axonal alignment. Briefly, after the standard fixation (4% PFA, 15 min, Sigma-Aldrich), blocking procedures (30 min, Sigma-Aldrich) and necessary washing (1× PBS, Sigma-Aldrich) steps, primary antibody (chicken polyclonal Neurofilament 200 kD antibody-abcam-1:500 dilution), 50 µl was added on the scaffolds and incubated overnight at 4 °C. The next day, after the washing steps with PBS, secondary antibody (Alexa 568 goat anti-chicken IgG-Molecular Probes-1:1000) 50 µl was added on the samples and incubated for 3 h at 4 °C. Finally, DAPI (Molecular Probes) nucleus staining was applied and immunofluorescence stained neural cells on the PLL-coated slides were imaged using a LSCM with 20× objective.[73]

SEM Analysis of Motor Neurons on the Scaffolds: SEM characterization of cultured motor neurons (with/without electrical stimulation) was performed for 72 h. SEM characterizations were carried out for only two various surface topography groups (S and G1-optimal channel width). In addition, SEM analysis was applied for all the surface coating groups (unmodified, gold nano decorated and PPy coated). Briefly, the fixation (2.5% glutaraldehyde, 30 min, +4 °C Sigma-Aldrich) and necessary washing procedures (PBS, 5 min) were applied. The samples were kept in increasing alcohol series (ethanol, 10–100%) for 5 min and dried at room temperature. The sputter coated cell-scaffold samples were characterized using SEM microscope.[126]

Quantification of Neural Cell Behaviors on the Film Scaffolds: The cell behaviors of motor neurons incubated on different neural scaffold material groups (with/without electrical stimulation) were quantitatively analyzed for three days. The behavioral studies were carried out based on the confocal data of NF-200 immunofluorescence staining for motor neurons. Following random selection of ten fields for each group, all the motor neurons in the area were analyzed. The deviation angles of the motor neuron axons from the grooves were measured by Image-J program for all the channeled neural scaffold groups.[73]

Preparation of the Tubular Nerve Guidance Conduits: Pre-implantation preparation processes of smooth surfaced (S) and G1 micro-channeled (ideal groove width, 1 µm) PCL/PLGA (10:1) scaffold materials were carried out. For this purpose, PCL/PLGA scaffold groups (PCL/PLGA S, PCL/PLGA G1, PCL/PLGA G1-BDNF/NGF, PCL/PLGA G1-BDNF/NGF-$AuNP_{50}$ and PCL/PLGA G1-BDNF/NGF-PPy) with 5 different features were prepared as mentioned above. All the film scaffolds include PDL/IKVAV pentapeptide surface coating as standard. The prepared film scaffolds were wrapped around a microneedle and formed into a tubular shape, then they were fixed with a biocompatible fibrin-based glue. All the tubular PCL/PLGA implant materials were prepared as standard with a length of 3 mm and a diameter of 1 mm. The prepared PCL/PLGA nerve guidance conduits (NGCs) were sterilized with UV light before implantation and stored at +4 °C.

Spinal Cord Injury, Surgical Procedures, and Scaffold Implantation: A total of 90 adult female Sprague Dawley rats (250–300 g) were used of this study. All the animal procedures were performed under Istanbul Medipol University, Institutional Animal Care and Use Committee (IMU-HADYEK). Apart from the five different experimental groups mentioned in the above section, the injured (SCI) but not NGCs implanted control group was also used. It was aimed to perform a right lateral hemisectional SCI injury model with a length of ≈3.5 mm in the T9-T10 region of the rat spinal cord. The animals were anesthetized using chloral hydrate at a dose of 400 mg k^{-1}g IP. First, the hairs in the thoracic region were shaved and the skin was disinfected with an iodine solution. The muscles were similarly opened by taking T9-T10 as the center and fixed to the sides. A laminectomy was performed at T9-T10 to allow 3.5 mm right lateral hemisection for NGC implantation by keeping the spine between T8-T11 stable, during which micro-aspiration was performed. After the designed NGCs were implanted in the gap regions, the injured regions were closed and sutured. Post-operative care was applied to the animals after surgical procedures for 2 weeks. After surgery, all the animals were given an antibiotic injection Baytril (enrofloxacin 2.5 mg k^{-1}g) once per day for 7 days and lactate ringer solution (5 mL/100 g) for 5 days. The bladders of the rats with SCI were expressed manually twice daily to eliminate urine inside the bladder until function recovered. After postoperative care, animals were kept in cages belonging to their group for a maximum of 10 weeks.

The Behavioral Analysis (BBB Tests): Two independent observers who were blinded to experimental groups tested the ability of the SD rats to move their hind limbs on open-field locomotion (BBB scale) in different weeks (2, 4, 6, 8, and 10 weeks) after implantation. In this test, there was a scale in the range of 0–21 and as a result of the values given, the mean scores at different time periods were determined for all the animals in each group. In the BBB scoring, "0" represents complete paralysis and "21" represents normal motor function.[127] Statistical analysis was performed by using SPSS Statistics 22 software and One-way analysis of variance (ANOVA-Tukey post-hoc analysis) was performed to determine inter-group differences ($p < 0.05$). $n = 3$, Data were represented as mean ± SD.

Spinal Cord Histology Studies: Hematoxylin & eosin (H&E) and Masson's trichrome staining protocols were used for general histological analysis of the spinal cords. In addition, immunohistological (IHC) fluorescent analyses were performed. For this purpose, SD rats under normal maintenance conditions were sacrificed for each experimental group at the end of the 5th and 10th weeks from implantation. First, euthanasia was performed using CO_2 by short breathing for a few minutes. Then, the back skin was opened quickly, and the muscle/bone tissues were removed, making the spinal cord segment in the injured area visible. A sample of ≈1 cm long spinal cord tissue containing the damaged area was taken and quickly placed in 10% formalin solution (Tekkim). For the dehydration process, the SC tissues were kept at 60 °C in the increasing ethanol (Sigma-Aldrich) series (from 70% to 100%); Subsequently, transparency was applied with two xylene (Tekkim) exchanges and the tissues were left at room temperature for 1 h. Then the tissue samples were embedded in paraffin (Tekkim) blocks, sectioned into 5 µm slices in the longitudinal direction and stained with H&E (Bio-Optica) for general histological examinations. In addition, collagen accumulations in the tissues were evaluated by Masson's trichrome staining (abcam).

Longitudinal SC sections from SD rats were IHC (immunohistochemistry) fluorescent stained using the following primary antibodies to detect axons (mouse β-III-tubulin, abcam, 1:500 dilution), neurofilaments (chicken Neurofilament 200 kD, abcam, 1:1000 dilution), astrocytes (mouse glial fibrillary acidic protein-GFAP, abcam, 1:100 dilution), microglia (mouse Iba1, abcam, 1:100 dilution), myelin basic proteins (mouse MBP, abcam, 1:200 dilution), nerve growth associated proteins (rabbit GAP-43, abcam, 1:400 dilution), macrophages (mouse CD68, abcam, 1:400 dilution), Schwann cells (rabbit S-100 beta, abcam, 1:400 dilution), oligodendrocytes (rabbit oligodendrocyte, abcam, 1:1000 dilution), motor neurons (mouse calcitonin gene related peptide-CGRP, abcam, 1:500 dilution). For IHC fluorescence staining, the SC sections on

PLL-coated slides were incubated at 60 °C for 45 min. After incubation of the SC sections in toluene solution (Tekkim) for 30 min., they were kept in decreasing ethanol series (100%, 96%, 80%, 70%) for 2 min. After washing steps two times with distilled water, the sections were washed with 0.1% Triton-X/PBS for 2 × 5 min. They were boiled in citrate buffer (10 mM, pH:6, Sigma-Aldrich) to perform antigen retrieval procedure for primary antibodies using a microwave oven (600 Watt) for 3 × 5 min. After washing steps two times with 0.1% Triton-X/PBS, 100 microliters of blocking solution (containing; 0.1% BSA, 0.1% Triton-X and 10% goat serum in PBS) were added to the SC sections. After 1 h of incubation (at RT) in the humidity chamber, the relevant primary antibodies were added on the SC sections and they were incubated overnight at +4 °C. The next day, suitable secondary antibodies (Alexa Fluor 488 goat-anti-mouse, Alexa Fluor 594 goat-anti-rabbit, Alexa Fluor 594 goat-anti-chicken, Invitrogen, 1:500 dilution) were added on the SC sections and kept in the dark conditions in a humidity chamber for 1 h. After three 0.1% Triton-X/PBS washing steps, the SC sections were stained with DAPI blue dye (Molecular Probes) and covered with coverslip using FluorSave Reagent (Sigma-Aldrich). All the prepared SC tissue samples were imaged using a laser scanning confocal microscope (LSCM, Zeiss LSM 780) with 20× objective.

Western Blotting: For this purpose, SD rats under normal maintenance conditions were sacrificed for each experimental group at the end of the 5th and 10th weeks from implantation as described in the related section, the SC tissue sample containing only the injury site (T9-T10 region) was taken and quickly dissected on ice. The SC tissue segment was degraded in RIPA buffer (RIPA Lysis and Extraction Buffer, Thermo Fisher) containing proteinase inhibitor cocktail (Halt Protease & Phosphatase Inhibitor, Thermo Fisher) for 2 h on ice. Then, the lysates were centrifuged (12.000 rpm, +4 °C) for 30 min., and the supernatants were collected. Protein concentrations in the samples were measured in a spectrophotometer using the BCA assay (Pierce BCA Protein Assay Kit, Thermo Fisher) and the concentrations were standardized for each group. The samples were subjected to SDS polyacrylamide gel electrophoresis (Thermo Fisher) and the separated proteins were transferred to a nitrocellulose membrane (Thermo Fisher). Then, the membranes were blocked with TBS containing 0.05% Tween-20 and 5% BSA for 1 h. Primary antibodies (rabbit anti-GFAP 1:1000 dilution-abcam, mouse anti-β-III-tubulin 1:1000 dilution-abcam, rabbit anti-beta tubulin 1:1000 dilution-abcam control) were added and the samples were kept at +4 °C for 5 h. After TBS washing step, suitable HRP conjugated secondary antibodies (anti-mouse 1:1000 dilution-abcam, anti-rabbit 1:1000 dilution-abcam) were added and the samples were incubated for 2 h. An ECL kit (Bio-Rad) was used to enhance chemiluminescence assay. The bands were visualized using an imaging system (Thermo Fisher) and the optical density of each band was calculated by using Image J software. Statistical analysis was performed by using SPSS Statistics 22 software and One-way analysis of variance (ANOVA-Tukey post-hoc analysis) was performed to determine inter-group differences ($p < 0.05$). n = 3, Data were represented as mean ± SD.

Statistical Analysis: All the experiments were carried out in triplicate and statistical analyses were performed using SPSS Statistics 22 software. One Way-ANOVA (Tukey post-hoc analysis) with the p-value of ˂ 0.05 was used to determine the statistical significance between study groups. n = 3, Data were represented as mean ± SD.

Supporting Information

Supporting Information is available from the Wiley Online Library or from the author.

Acknowledgements

The authors would like to thank The Scientific and Technological Research Council of Turkey (TUBITAK, Grant no: 119S141) for providing financial support to this project.

Conflict of Interest

The authors declare no conflict of interest.

Data Availability Statement

The data that support the findings of this study are available from the corresponding author upon reasonable request.

Keywords

gold nanoparticles, nerve guidance conduit, neural tissue engineering, neuronal regeneration, polycaprolactone/poly-lactic-glycolic acid, spinal cord injury

Received: October 4, 2023
Revised: December 22, 2023
Published online: January 18, 2024

[1] M. Khorasanizadeh, M. Yousefifard, M. Eskian, Y. Lu, M. Chalangari, J. S. Harrop, S. B. Jazayeri, S. Seyedpour, B. Khodaei, M. Hosseini, V. Rahimi-Movaghar, *J. Neurosurg. Spine* **2019**, *30*, 683.
[2] W. Q. Gong, T. H. Zhang, M. X. Che, Y. J. Wang, C. Y. He, L. D. Liu, Z. S. Lv, C. S. Xiao, H. Wang, S. K. Zhang, *Mater Today Bio* **2023**, *18*, 100524.
[3] H. Tabesh, G. Amoabediny, N. S. Nik, M. Heydari, M. Yosefifard, S. O. R. Siadat, K. Mottaghy, *Neurochem. Int.* **2009**, *54*, 73.
[4] B. Battiston, I. Papalia, P. Tos, S. Geuna, *Int. Rev. Neurobiol.* **2009**, *87*, 1.
[5] A. Buss, G. A. Brook, B. Kakulas, D. Martin, R. Franzen, J. Schoenen, J. Noth, A. B. Schmitt, *Brain* **2004**, *127*, 34.
[6] C. E. Schmidt, J. B. Leach, *Annu. Rev. Biomed. Eng.* **2003**, *5*, 293.
[7] E. O. Johnson, P. N. Soucacos, *Injury* **2008**, *39*, 30.
[8] S. Panseri, C. Cunha, J. Lowery, U. Del Carro, F. Taraballi, S. Amadio, A. Vescovi, F. Gelain, *BMC Biotechnol.* **2008**, *8*, 39.
[9] M. Y. Lin, G. Manzano, R. Gupta, *Hand Clin.* **2013**, *29*, 331.
[10] S. E. Mackinnon, V. B. Doolabh, C. B. Novak, E. P. Trulock, *Plast. Reconstr. Surg.* **2001**, *107*, 1419.
[11] S. A. Barbour, W. King, *Am. J. Sports Med.* **2003**, *31*, 791.
[12] D. Muir, *Exp. Neurol.* **2010**, *223*, 102.
[13] J. M. Griffin, F. Bradke, *EMBO Mol. Med.* **2020**, *12*, 11505.
[14] C. S. Ahuja, J. R. Wilson, S. Nori, M. R. N. Kotter, C. Druschel, A. Curt, M. G. Fehlings, *Nat. Rev. Dis. Primers* **2017**, *3*, 17018.
[15] P. Sensharma, G. Madhumathi, R. D. Jayant, A. K. Jaiswal, *Mater. Sci. Eng., C* **2017**, *77*, 1302.
[16] S. M. Willerth, S. E. Sakiyama-Elbert, *Adv. Drug Deliv. Rev.* **2007**, *59*, 325.
[17] A. Subramanian, U. M. Krishnan, S. Sethuraman, *J Biomed Sci* **2009**, *16*, 108.
[18] F. J. O'Brien, *Mater. Today* **2011**, *14*, 88.
[19] C.-Y. Yang, W.-Y. Huang, L.-H. Chen, N.-W. Liang, H.-C. Wang, J. Lu, X. Wang, T.-W. Wang, *J. Mater. Chem. B* **2021**, *9*, 567.
[20] D. Sirkkunan, B. Pingguan-Murphy, F. Muhamad, *Gels* **2022**, *8*, 25.
[21] S. Chanet, A. C. Martin, *Prog. Mol. Biol. Transl. Sci.* **2014**, *126*, 317.
[22] Y. Li, T. Dong, Z. Li, S. Ni, F. Zhou, O. A. Alimi, S. Chen, B. Duan, M. Kuss, S. Wu, *Mater. Today Chem.* **2022**, *24*, 100944.
[23] Y. Dai, W. Wang, X. Zhou, L. li, Y. Tang, M. Shao, F. Lyu, *ACS Appl. Nano Mater.* **2023**, *6*, 5980.
[24] L. U. Vinzons, S.-P. Lin, *ACS Appl. Nano Mater.* **2022**, *5*, 6935.
[25] J. Litowczenko, J. K. Wychowaniec, K. Załęski, Ł. Marczak, C. J. C. Edwards-Gayle, K. Tadyszak, B. M. Maciejewska, *Biomater. Adv.* **2023**, *154*, 213653.

[26] S. Tortorella, P. Greco, F. Valle, M. Barbalinardo, G. Foschi, F. Lugli, M. Dallavalle, F. Zerbetto, C. A. Bortolotti, F. Biscarini, *Bioprinting* **2022**, *26*, e00194.
[27] N. Y. Patrawalla, R. Raj, V. Nazar, V. Kishore, *Tissue Eng., Part B* **2023**.
[28] S. Song, Y. Li, J. Huang, S. Cheng, Z. Zhang, *Biomater. Adv.* **2023**, *148*, 213385.
[29] H. Patel, M. Bonde, G. Srinivasan, *Trends in Biomaterials and Artificial Organs* **2011**, *25*, 20.
[30] M. Okada, *Prog. Polym. Sci.* **2002**, *27*, 87.
[31] L. S. Nair, C. T. Laurencin, *Prog. Polym. Sci.* **2007**, *32*, 762.
[32] L. Ghasemi-Mobarakeh, M. P. Prabhakaran, M. Morshed, M.-H. Nasr-Esfahani, S. Ramakrishna, *Biomaterials* **2008**, *29*, 4532.
[33] D. Gupta, J. Venugopal, M. P. Prabhakaran, V. R. G. Dev, S. Low, A. T. Choon, S. Ramakrishna, *Acta Biomater.* **2009**, *5*, 2560.
[34] L. Ghasemi-Mobarakeh, M. P. Prabhakaran, M. Morshed, M. H. Nasr-Esfahani, S. Ramakrishna, *Mater. Sci. Eng., C* **2010**, *30*, 1129.
[35] J. Bockelmann, K. Klinkhammer, A. von Holst, N. Seiler, A. Faissner, G. A. Brook, D. Klee, J. Mey, *Tissue Eng., Part A* **2011**, *17*, 475.
[36] A. Cooper, N. Bhattarai, M. Q. Zhang, *Carbohydr. Polym.* **2011**, *85*, 149.
[37] V. Mahairaki, S. H. Lim, G. T. Christopherson, L. Y. Xu, I. Nasonkin, C. Yu, H. Q. Mao, V. E. Koliatsos, *Tissue Eng., Part A* **2011**, *17*, 855.
[38] M. F. B. Daud, K. C. Pawar, F. Claeyssens, A. J. Ryan, J. W. Haycock, *Biomaterials* **2012**, *33*, 5901.
[39] J. W. Xie, W. Y. Liu, M. R. MacEwan, P. C. Bridgman, Y. N. Xia, *ACS Nano* **2014**, *8*, 1878.
[40] W. Zhu, F. Masood, J. O'Brien, L. G. Zhang, *Nanomed-Nanotechnol* **2015**, *11*, 693.
[41] K. Baranes, M. Shevach, O. Shefi, T. Dvir, *Nano Lett.* **2016**, *16*, 2916.
[42] S. J. Lee, M. Nowicki, B. Harris, L. G. Zhang, *Tissue Eng., Part A* **2017**, *23*, 491.
[43] I. Tonazzini, M. Moffa, D. Pisignano, M. Cecchini, *Nanotechnology* **2017**, *28*, 155303.
[44] L. L. Huang, L. Zhu, X. W. Shi, B. Xia, Z. Y. Liu, S. Zhu, Y. F. Yang, T. Ma, P. Z. Cheng, K. Luo, J. H. Huang, Z. J. Luo, *Acta Biomater.* **2018**, *68*, 223.
[45] H. R. Lin, C. J. Kuo, C. Y. Yang, S. Y. Shaw, Y. J. Wu, *J. Biomed. Mater. Res.* **2002**, *63*, 271.
[46] J. Jagur-Grodzinski, *React. Funct. Polym.* **1999**, *39*, 99.
[47] L. Yao, S. G. Wang, W. J. Cui, R. Sherlock, C. O'Connell, G. Damodaran, A. Gorman, A. Windebank, A. Pandit, *Acta Biomater.* **2009**, *5*, 580.
[48] C. Binder, V. Milleret, H. Hall, D. Eberli, T. Luhmann, *J. Biomed. Mater. Res., Part B* **2013**, *101*, 1200.
[49] S. K. Choi, J. K. Park, K. M. Lee, S. K. Lee, W. B. Jeon, *J. Biomed. Mater. Res., Part B* **2013**, *101*, 1329.
[50] F. Zamani, M. Amani-Tehran, M. Latifi, M. A. Shokrgozar, A. Zaminy, *J. Biomed. Mater. Res., Part A* **2014**, *102*, 506.
[51] A. Raspa, A. Marchini, R. Pugliese, M. Mauri, M. Maleki, R. Vasitad, F. Gelain, *Nanoscale* **2016**, *8*, 253.
[52] D. Angelaki, P. Kavatzikidou, C. Fotakis, E. Stratakis, A. Ranella, *Tissue Eng. Regen. Med.* **2023**, *20*, 111.
[53] H. Liu, P. Lv, Y. Zhu, H. Wu, K. Zhang, F. Xu, L. Zheng, J. Zhao, *Sci. Rep.* **2017**, *7*, 39869.
[54] S. Zhang, H. Yan, J.-M. Yeh, X. Shi, P. Zhang, *Macromol. Biosci.* **2019**, *19*, 1900147.
[55] N. Nazeri, R. Karimi, H. Ghanbari, *J. Biomed. Mater. Res., Part A* **2021**, *109*, 159.
[56] N. A. Aval, R. Emadi, A. Valiani, M. Kharaziha, M. Karimipour, R. Rahbarghazi, *Composites, Part B* **2019**, *173*, 106863.
[57] R. Seyedebrahimi, S. Razavi, J. Varshosaz, E. Vatankhah, M. Kazemi, *J. Cluster Sci.* **2021**, *32*, 631.
[58] C. Y. Wang, K. H. Zhang, C. Y. Fan, X. M. Mo, H. J. Ruan, F. F. Li, *Acta Biomater.* **2011**, *7*, 634.
[59] S. Y. Chew, R. Mi, A. Hoke, K. W. Leong, *Biomaterials* **2008**, *29*, 653.
[60] M. H. Lin, L. Yang, R. Fu, H. Y. Zhao, *J. Huazhong Univ. Sci. Technol. [Med. Sci.]* **2008**, *28*, 513.
[61] L. Zhang, H. Jiang, Z. Q. Hu, *Stem Cells Dev.* **2011**, *20*, 1723.
[62] Q. Q. Han, W. J. Sun, H. Lin, W. X. Zhao, Y. Gao, Y. N. Zhao, B. Chen, Z. F. Xiao, W. Hu, Y. Li, B. Yang, J. W. Dai, *Tissue Eng., Part A* **2009**, *15*, 2927.
[63] N. Weishaupt, A. Blesch, K. Fouad, *Exp. Neurol.* **2012**, *238*, 254.
[64] A. D. Lander, *Trends Neurosci.* **1989**, *12*, 189.
[65] H. Shin, S. Jo, A. G. Mikos, *Biomaterials* **2003**, *24*, 4353.
[66] M. F. Brizzi, G. Tarone, P. Defilippi, *Curr. Opin. Cell Biol.* **2012**, *24*, 645.
[67] S. Patel, K. Kurpinski, R. Quigley, H. F. Gao, B. S. Hsiao, M. M. Poo, S. Li, *Nano Lett.* **2007**, *7*, 2122.
[68] D. N. Adams, E. Y. C. Kao, C. L. Hypolite, M. D. Distefano, W. S. Hu, P. C. Letourneau, *J. Neurobiol.* **2005**, *62*, 134.
[69] Y. T. Wei, W. M. Tian, X. Yu, F. Z. Cui, S. P. Hou, Q. Y. Xu, I. S. Lee, *Biomed. Mater.* **2007**, *2*, S142.
[70] Z. W. Zou, Q. X. Zheng, Y. C. Wu, W. Song, B. Wu, *Materials Science & Engineering C-Materials for Biological Applications* **2009**, *29*, 2099.
[71] H. Xie, J. Li, L. Li, Y. Dong, G. Q. Chen, K. C. Chen, *Acta Biomater.* **2013**, *9*, 7845.
[72] T. H. Huang, Y. Pei, D. Zhang, Y. F. Li, K. A. Kilian, *Nanoscale* **2016**, *8*, 10891.
[73] A. Aydeger, N. Aysit, G. Baydas, C. Cakici, U. C. Erim, M. D. Arpa, I. Ozcicek, *Biomater. Adv.* **2023**, *152*, 213472.
[74] M. H. Kang, K. H. Cheon, K. I. Jo, J. H. Ahn, H. E. Kim, H. D. Jung, T. S. Jang, *Mater Design* **2020**, *196*, 109182.
[75] Y. Z. Qian, H. B. Chen, Y. Xu, J. X. Yang, X. F. Zhou, F. M. Zhang, N. Gu, *Int. J. Nanomed.* **2016**, *11*, 5057.
[76] T. H. Nguyen, B. T. Lee, *J. Mater. Sci.-Mater. M* **2010**, *21*, 1969.
[77] K. Li, S. P. Zhang, S. Y. Wang, F. N. Zhu, M. L. Liu, X. N. Gu, P. Li, Y. B. Fan, *J. Biomed. Nanotechnol.* **2019**, *15*, 477.
[78] X. M. Feng, H. P. Huang, Q. Q. Ye, J. J. Zhu, W. H. Hou, *J. Phys. Chem. C* **2007**, *111*, 8463.
[79] J. J. Xu, J. C. Hu, B. G. Quan, Z. X. Wei, *Macromol Rapid Commun.* **2009**, *30*, 936.
[80] C. E. Hulsebosch, *Adv. Physiol. Educ.* **2002**, *26*, 238.
[81] J. Y. Tyler, X. M. Xu, J. X. Cheng, *Nanoscale* **2013**, *5*, 8821.
[82] S. Couillard-Després, L. Bieler, Eds: N. Weidner, R. Rupp, K.E. Tansey, *Neurological Aspects of Spinal Cord Injury*, Springer International Publishing, Cham, **2017**, 503.
[83] A. Alizadeh, S. M. Dyck, S. Karimi-Abdolrezaee, *Front Neurol* **2019**, *10*, 282.
[84] N. Hejrati, M. G. Fehlings, *Curr. Opin. Pharmacol.* **2021**, *60*, 331.
[85] M. G. Fehlings, J. R. Wilson, L. A. Tetreault, B. Aarabi, P. Anderson, P. M. Arnold, D. S. Brodke, A. S. Burns, K. Chiba, J. R. Dettori, J. C. Furlan, G. Hawryluk, L. T. Holly, S. Howley, T. Jeji, S. Kalsi-Ryan, M. Kotter, S. Kurpad, B. K. Kwon, R. J. Marino, A. R. Martin, E. Massicotte, G. Merli, J. W. Middleton, H. Nakashima, N. Nagoshi, K. Palmieri, A. C. Skelly, A. Singh, E. C. Tsai, et al., *Global Spine J.* **2017**, *7*, 203S.
[86] J. C. T. Chio, J. Wang, V. Surendran, L. Li, M.-M. Zavvarian, K. Pieczonka, M. G. Fehlings, *Neurobiol. Dis.* **2021**, *148*, 105187.
[87] K. Kamiya, M. Koda, T. Furuya, K. Kato, H. Takahashi, T. Sakuma, T. Inada, M. Ota, S. Maki, A. Okawa, Y. Ito, K. Takahashi, M. Yamazaki, *Eur. Spine J.* **2015**, *24*, 963.
[88] S. Casha, D. Zygun, M. D. McGowan, I. Bains, V. W. Yong, R. J. Hurlbert, *Brain* **2012**, *135*, 1224.
[89] R. G. Grossman, M. G. Fehlings, R. F. Frankowski, K. D. Burau, D. S. Chow, C. Tator, A. Teng, E. G. Toups, J. S. Harrop, B. Aarabi, C. I. Shaffrey, M. M. Johnson, S. J. Harkema, M. Boakye, J. D. Guest, J. R. Wilson, *J. Neurotrauma* **2014**, *31*, 239.

[90] K. Kucher, D. Johns, D. Maier, R. Abel, A. Badke, H. Baron, R. Thietje, S. Casha, R. Meindl, B. Gomez-Mancilla, C. Pfister, R. Rupp, N. Weidner, A. Mir, M. E. Schwab, A. Curt, *Neurorehabil. Neural Repair* **2018**, *32*, 578.
[91] N. Forgione, M. G. Fehlings, *World Neurosurg.* **2014**, *82*, e535.
[92] A. J. Mothe, N. G. Tassew, A. P. Shabanzadeh, R. Penheiro, R. J. Vigouroux, L. Huang, C. Grinnell, Y. F. Cui, E. Fung, P. P. Monnier, B. K. Mueller, C. H. Tator, *Sci. Rep.* **2017**, *7*, 10529.
[93] C. M. Zipser, J. J. Cragg, J. D. Guest, M. G. Fehlings, C. R. Jutzeler, A. J. Anderson, A. Curt, *Lancet Neurol.* **2022**, *21*, 659.
[94] B. Fan, Z. Wei, S. Feng, *Bone Res.* **2022**, *10*, 35.
[95] Q. Z. Zhang, B. Shi, J. X. Ding, L. S. Yan, J. P. Thawani, C. F. Fu, X. S. Chen, *Acta Biomater.* **2019**, *88*, 57.
[96] M. Tsintou, K. Dalamagkas, A. M. Seifalian, *Neural Regen. Res.* **2015**, *10*, 726.
[97] W. A. Abbas, M. E. Ibrahim, M. El-Naggar, W. A. Abass, I. H. Abdullah, B. I. Awad, N. K. Allam, *ACS Biomater. Sci. Eng.* **2020**, *6*, 6490.
[98] R. B. Shultz, Y. Zhong, *Neural Regen. Res.* **2021**, *16*, 247.
[99] L. Li, B. Xiao, J. Mu, Y. Zhang, C. Zhang, H. Cao, R. Chen, H. K. Patra, B. Yang, S. Feng, Y. Tabata, N. K. H. Slater, J. Tang, Y. Shen, J. Gao, *ACS Nano* **2019**, *13*, 14283.
[100] R. Ji, Z. Hao, H. Wang, X. Li, L. Duan, F. Guan, S. Ma, *Gels* **2023**, *9*, 907.
[101] A. Chakraborty, A. J. Ciciriello, C. M. Dumont, R. M. Pearson, *AAPS PharmSciTech* **2021**, *22*, 101.
[102] H. Shen, B. Xu, C. Yang, W. Xue, Z. You, X. Wu, D. Ma, D. Shao, K. Leong, J. Dai, *Biomaterials* **2022**, *280*, 121279.
[103] E. J. Roh, D. S. Kim, J. H. Kim, C. S. Lim, H. Choi, S. Y. Kwon, S. Y. Park, J. Y. Kim, H. M. Kim, D. Y. Hwang, D. K. Han, I. Han, *Biomaterials* **2023**, *299*, 122160.
[104] S. Song, J. Zhou, J. Wan, X. Zhao, K. Li, C. Yang, C. Zheng, L. Wang, Y. Tang, C. Wang, J. Liu, *Int. J. Bioprint.* **2023**, *9*, 692.
[105] F. He, K. Cheng, J. Qi, F. He, C. Chu, Y. Xiong, J. Zhao, J. Ding, F. Kong, Z. Cao, G. Liu, W. Deng, *Chem. Eng. J.* **2023**, *472*, 144977.
[106] B. W. Tuft, S. F. Li, L. J. Xu, J. C. Clarke, S. P. White, B. A. Guymon, K. X. Perez, M. R. Hansen, C. A. Guymon, *Biomaterials* **2013**, *34*, 42.
[107] H. Cheng, L. H. Zhou, B. H. Li, M. Zhu, H. P. Too, W. K. Choi, *Nanomed-Nanotechnol* **2014**, *10*, 1871.
[108] S. Gilles, S. Winter, K. E. Michael, S. H. Meffert, P. G. Li, K. Greben, U. Simon, A. Offenhausser, D. Mayer, *Small* **2012**, *8*, 3357.
[109] F. Pan, M. Zhang, G. M. Wu, Y. K. Lai, B. Greber, H. R. Scholer, L. F. Chi, *Biomaterials* **2013**, *34*, 8131.
[110] M. Moffa, A. G. Sciancalepore, L. G. Passione, D. Pisignano, *Small* **2014**, *10*, 2439.
[111] K. Yang, H. Jung, H. R. Lee, J. S. Lee, S. R. Kim, K. Y. Song, E. Cheong, J. Bang, S. G. Im, S. W. Cho, *ACS Nano* **2014**, *8*, 7809.
[112] N. Gomez, Y. Lu, S. C. Chen, C. E. Schmidt, *Biomaterials* **2007**, *28*, 271.
[113] G. Dos Reis, F. Fenili, A. Gianfelice, G. Bongiorno, D. Marchesi, P. E. Scopelliti, A. Borgonovo, A. Podesta, M. Indrieri, E. Ranucci, P. Ferruti, C. Lenardi, P. Milani, *Macromol. Biosci.* **2010**, *10*, 842.
[114] R. Balint, N. J. Cassidy, S. H. Cartmell, *Acta Biomater.* **2014**, *10*, 2341.
[115] D. Shahriari, J. Y. Koffler, M. H. Tuszynski, W. M. Campana, J. S. Sakamoto, *Tissue Eng., Part A* **2017**, *23*, 415.
[116] N. A. Silva, R. A. Sousa, J. S. Fraga, M. Fontes, H. Leite-Almeida, R. Cerqueira, A. Almeida, N. Sousa, R. L. Reis, A. J. Salgado, *Tissue Eng., Part C* **2013**, *19*, 101.
[117] F. Gelain, S. Panseri, S. Antonini, C. Cunha, M. Donega, J. Lowery, F. Taraballi, G. Cerri, M. Montagna, F. Baldissera, A. Vescovi, *ACS Nano* **2011**, *5*, 227.
[118] A. M. Thomas, M. B. Kubilius, S. J. Holland, S. K. Seidlits, R. M. Boehler, A. J. Anderson, B. J. Cummings, L. D. Shea, *Biomaterials* **2013**, *34*, 2213.
[119] K. M. Keefe, I. S. Sheikh, G. M. Smith, *Int. J. Mol. Sci.* **2017**, *18*, 548.
[120] R. D. Almeida, B. J. Manadas, C. V. Melo, J. R. Gomes, C. S. Mendes, M. M. Graos, R. F. Carvalho, A. P. Carvalho, C. B. Duarte, *Cell Death Differ.* **2005**, *12*, 1329.
[121] M. Sasaki, C. Radtke, A. M. Tan, P. Zhao, H. Hamada, K. Houkin, O. Honmou, J. D. Kocsis, *J. Neurosci.* **2009**, *29*, 14932.
[122] S. F. Han, B. Wang, W. Jin, Z. F. Xiao, X. Li, W. Y. Ding, M. Kapur, B. Chen, B. Y. Yuan, T. S. Zhu, H. D. Wang, J. Wang, Q. Dong, W. B. Liang, J. W. Dai, *Biomaterials* **2015**, *41*, 89.
[123] J. Turkevich, P. C. Stevenson, J. Hillier, *Discuss. Faraday Soc.* **1951**, *11*, 55.
[124] S. D. Perrault, W. C. W. Chan, *J. Am. Chem. Soc.* **2009**, *131*, 17042.
[125] I. Ozcicek, N. Aysit, C. Cakici, A. Aydeger, *Materials Science & Engineering C-Materials for Biological Applications* **2021**, *128*, 112308.
[126] I. Ozcicek, N. Aysit, C. Cakici, N. U. Ayturk, A. Aydeger, U. C. Erim, *Adv. Mater. Interfaces* **2022**, 9.
[127] D. M. Basso, M. S. Beattie, J. C. Bresnahan, *J. Neurotrauma* **1995**, *12*, 1.